Review

Novel Structures and Applications of Graphene-Based Semiconductor Photocatalysts: Faceted Particles, Photonic Crystals, Antimicrobial and Magnetic Properties

Marcin Janczarek [1], Maya Endo-Kimura [2], Zhishun Wei [3], Zuzanna Bielan [4], Tharishinny R. Mogan [2], Tamer M. Khedr [2,5], Kunlei Wang [2,6], Agata Markowska-Szczupak [7] and Ewa Kowalska [2,*]

1 Faculty of Chemical Technology, Institute of Chemical Technology and Engineering, Poznan University of Technology, 60-965 Poznan, Poland; marcin.janczarek@put.poznan.pl
2 Institute for Catalysis (ICAT), Hokkaido University, Sapporo 001-0021, Japan; m_endo@cat.hokudai.ac.jp (M.E.-K.); rajamogan.t@cat.hokudai.ac.jp (T.R.M.); tamerkhedr56@gmail.com (T.M.K.); kunlei@cat.hokudai.ac.jp (K.W.)
3 Hubei Provincial Key Laboratory of Green Materials for Light Industry, Hubei University of Technology, Wuhan 430068, China; wei.zhishun@hbut.edu.cn
4 Department of Process Engineering and Chemical Technology, Chemical Faculty, Gdansk University of Technology, 80-233 Gdansk, Poland; bielan_chan@onet.eu
5 Nanomaterials and Nanotechnology Department, Central Metallurgical Research and Development Institute (CMRDI), P.O. Box. 87 Helwan, Cairo 11421, Egypt
6 Northwest Research Institute, Co. Ltd., Lanzhou 730000, China
7 Department of Chemical and Process Engineering, West Pomeranian University of Technology in Szczecin, Al. Piastów 42, 71-065 Szczecin, Poland; agata@erb.pl
* Correspondence: kowalska@cat.hokudai.ac.jp

Abstract: Graphene, graphene oxide, reduced graphene oxide and their composites with various compounds/materials have high potential for substantial impact as cheap photocatalysts, which is essential to meet the demands of global activity, offering the advantage of utilizing "green" solar energy. Accordingly, graphene-based materials might help to reduce reliance on fossil fuel supplies and facile remediation routes to achieve clean environment and pure water. This review presents recent developments of graphene-based semiconductor photocatalysts, including novel composites with faceted particles, photonic crystals, and nanotubes/nanowires, where the enhancement of activity mechanism is associated with a synergistic effect resulting from the presence of graphene structure. Moreover, antimicrobial potential (highly needed these days), and facile recovery/reuse of photocatalysts by magnetic field have been addresses as very important issue for future commercialization. It is believed that graphene materials should be available soon in the market, especially because of constantly decreasing prices of graphene, vis response, excellent charge transfer ability, and thus high and broad photocatalytic activity against both organic pollutants and microorganisms.

Keywords: graphene; heterogeneous photocatalysis; antimicrobial properties; photonic crystals; magnetic particles; vis response; catalyst recovery; environmental purification; composite photocatalysts

1. Introduction

Graphene, one of carbon allotropes, consists of a single layer of atoms arranged in a two-dimensional (2D) honeycomb lattice by a σ-bond. Each carbon atom, connected to three nearest ones, contributes one electron to a conduction band, resulting in a semimetal nature of graphene, which causes efficient electricity/heat conductivity along its sheet. Moreover, graphene absorbs light of all visible range of solar spectrum. Its unique chemical, physical, and mechanical properties are extraordinary and, thus, graphene is considered as most promising material in nanomaterial science. Accordingly, graphene (G), graphene oxide (GO) and reduced graphene oxides (rGO) have been intensively examined for various possible applications, including electronics (transistors, transparent conducting

electrodes, optoelectronics, quantum dots), light processing, energy conversion (fuel and solar cells), energy storage (supercapacitor, batteries), sensors, environmental purification (filter, adsorbent), plasmonics, catalysis, and photocatalysis.

Recently, the research on photocatalysis has been highly exploring due to the possibility to use "green energy" (the sun) to drive many photochemical reactions, e.g., water splitting, photocurrent generation, water and air purification, wastewater treatment, disinfections, self-cleaning and synthesis of organic compounds. Among various semiconductor photocatalysts, titania (titanium(IV) oxide, TiO_2) is probably the most widely investigated due to high activity, stability, abundance, and low toxicity [1,2], but its application is limited due to charge carriers' recombination and inability of visible light (vis) absorption. In this regard, titania has been modified with different elements and species, including doping, surface modification and coupling [3]. Accordingly, G/GO/rGO has also been proposed for surface modification of titania (and other wide-bandgap semiconductors), due to large specific surface area (efficient reagents adsorption), high conductivity (inhibited charge carriers' recombination), flexible structure and high stability [4–6]. For example, hydrothermally prepared composites have shown to be quite efficient for photocatalytic decomposition of organic compounds, e.g., bisphenol A under both UV and vis irradiation (TiO_2-rGO) [7], 4-chlorophenol under solar radiation (TiO_2-G) [8], and butene in the gas phase (TiO_2-GO) [9]. TiO_2-rGO, synthesized by ionothermal [10] method and laser synthesis [11], is able to generate hydrogen under UV irradiation, indicating that graphene might work as co-catalyst on titania surface similar to well-known noble metals for hydrogen evolution. ZnO-G, synthesized by combined method of Hummers, Offeman and hydrothermal treatment, is efficient for degradation of cyanide in water under UV, vis, solar and even NIR irradiation due to plasmonic properties of graphene [12]. Moreover, CO_2 fixation and conversion into CH_3OH under vis irradiation is possible on α-Fe_2O_3-ZnO/rGO, prepared by the Hummer/redox replacement/electrochemical process [13]. Although the composites of G/GO/rGO/wide-bandgap semiconductors are widely investigated for various photocatalytic applications, the function of graphene has not been completely understood yet, as comprehensively summarized by Giovannetti et al. [14]. It has been proposed that electrons from conduction band (CB) of wide-bandgap semiconductor under UV irradiation migrate to graphene, due to its more positive Fermi level, and thus hindering recombination of photogenerated charge carriers (e^-/h^+), whereas the opposite direction of electron migration is expected under vis irradiation, i.e., from photoexcited state of graphene to CB of titania (similarly to plasmonic photocatalysis [15]).

Although the research on photocatalytic applications of graphene is quite new, many reports and even review papers have already been published on graphene-based photocatalytic materials. Accordingly, this review presents the most interesting and novel photocatalysts based on graphene, such as faceted particles, 2D nanostructures and photonic crystals. Moreover, antimicrobial properties and magnetically separable photocatalysts have been addressed as probably one of the most prospective applications of graphene-based photocatalysts.

2. Morphology Design of Graphene-Based Composites

2.1. The Composites of Graphene with Faceted Particles

Since the successful preparation of faceted anatase titania and demonstration of its exceptional photocatalytic properties [16,17], the attention on the particles with exposed high reactive facets and their role in the mechanism of photocatalysis is constantly growing [18–20]. To date, many research papers on this topic have been published. Most of them concern faceted TiO_2 [21–26], but the scientific reports about other types of photocatalysts with faceted morphology, such as Cu_2O [27,28], $BiVO_4$ [29,30], ZnO [31], $AgNbO_3$ [32], Ag_2MoO_4 [33] and BiOCl [34,35], are also available in the literature. For example, the morphology of anatase titania can be recognized as decahedron, octahedron, rod, belt and sheet structures. Some of these morphologies are enclosed with exposed facets such as (001), (101) and (010). The mentioned facets differ in the values of surface energy determining

the resultant character of activity (0.90 J m^{-2} for (001), 0.44 J m^{-2} for (101) and 0.53 J m^{-2} for (010)) [36]. The proper tuning of the ratio of different facets might influence the overall photocatalytic activity. In this relation, there is a still important challenge to prepare faceted particles with design ratio between facets.

The intrinsic property of graphene, i.e., high electron conductivity, influences the photocatalytic activity of semiconductor particles through interaction between graphene and semiconductor at the interfaces. Taking into consideration the photocatalysts in the form of faceted particles and their composites with graphene, one can expect the synergistic effect of high reactive facets and an enhancement of electron transfer process to improve photocatalytic activity. Jiang et al. started the research on TiO$_2$/G composites consisting of graphene and anatase with exposed (001) facets [37]. It has been proposed that the superior photocatalytic activity of prepared composites results from high charge separation rate because of an efficient electron transfer in the frame of semiconductor-graphene interface. Similarly, excellent activity has been reported by Zhao et al. on a novel core-shell-structure (G-wrapped Pt/TiO$_2$, Figure 1), in which anatase nanocrystals with co-exposed (001) and (101) facets improve the separation of photogenerated charges, and thus enhance the photocatalytic efficiency [38]. The wrapped rGO sheets as an efficient electron acceptor and transporter is not only one positive of graphene, but also the surface hydroxyl groups and extended π bonds are beneficial to enhance the adsorption and activation of reagents, e.g., CO$_2$. It has been proposed that rGO(shell)-Pt-TiO$_2$(core) ternary composites might promote the vectorial electron transfer (TiO$_2$→Pt→rGO), enhancing the separation of charge carriers [38].
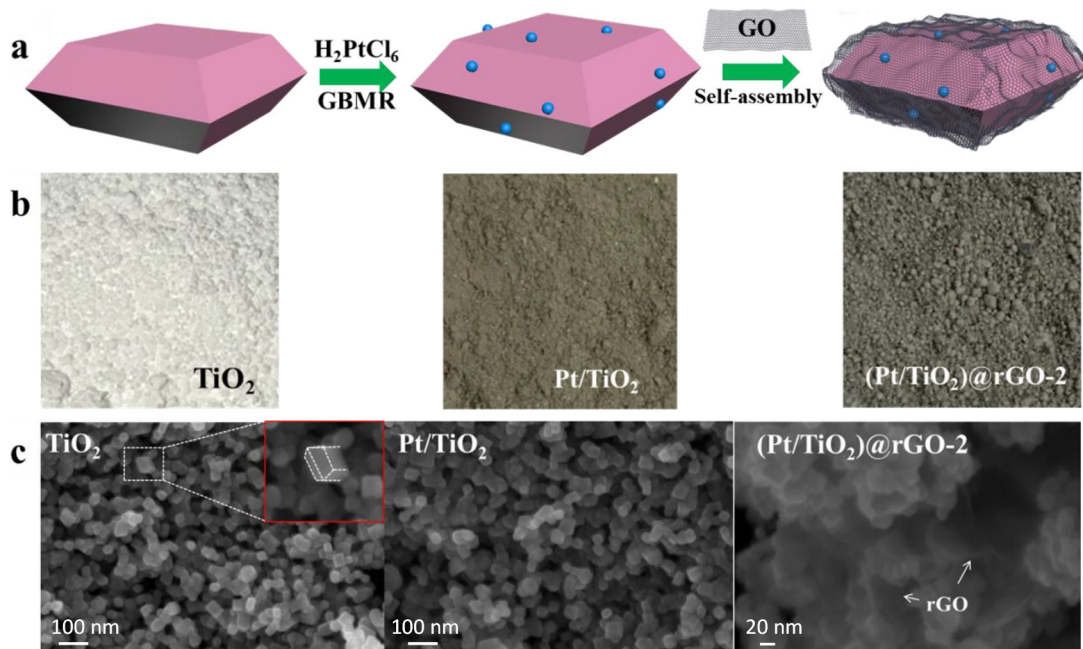
Figure 1. Preparation procedure and photographs of (Pt/TiO$_2$)@rGO photocatalysts: (**a**) the schematic graph for the two-step synthesis of supported Pt NPs and wrapping rGO shells on the surface of TiO$_2$ nanocrystals; (**b**) the digital photograph and (**c**) SEM images of TiO$_2$, Pt/TiO$_2$ and (Pt/TiO$_2$)@rGO. Reprinted with permission from [38] after slight modification. Copyright 2018 Elsevier.

Another promising interaction including additional presence of structural titania defects has been observed by Wang et al. [39]. The rGO-wrapped titania nanocrystals (TiO$_2$ NCs@RGO) with oxygen vacancies (Vo) and Ti^{3+} defects have been synthesized by electrostatically wrapping GO around TiO$_2$ NCs, following by thermal annealing at 400 °C (Figure 2). It has been found that the photocatalytic activity of TiO$_2$ NCs@RGO is 2.4 times higher than that of TiO$_2$ NCs for degradation of methyl orange. It has been proposed that

the improvement of photocatalytic activity is possibly caused by better charge separation at the interface of TiO$_2$ NCs and rGO layer, and enhanced optical absorption at vis range due to new donor levels inside titania bandgap, i.e., the defects, such as Vo and Ti^{3+} [39].
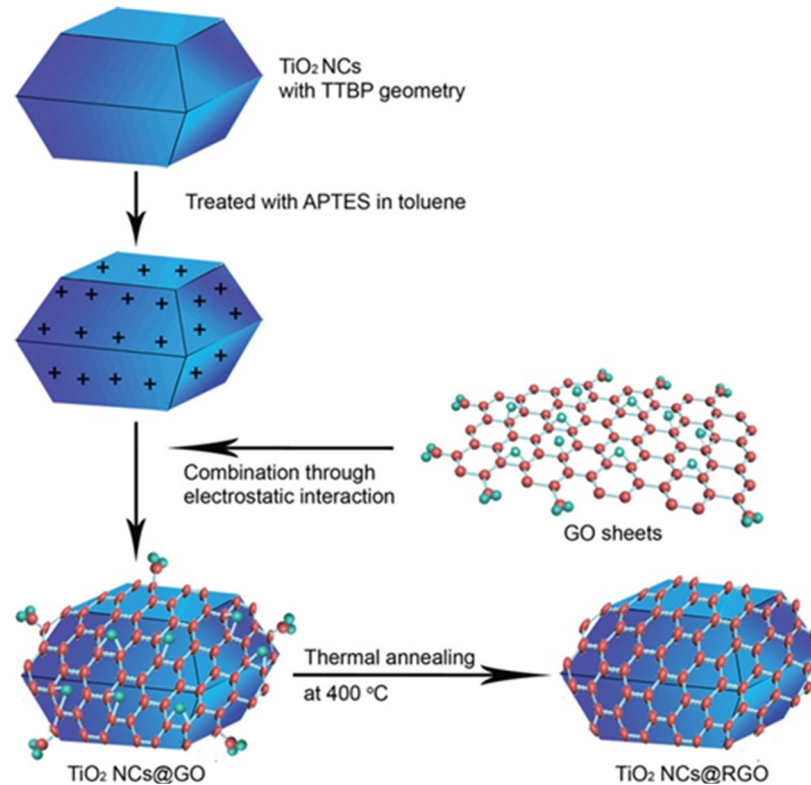
Figure 2. Schematic illustration for synthesis of TiO$_2$ NCs@RGO composites (RGO–rGO). Reprinted with permission from [39]. Copyright 2014 John Wiley and Sons.

Liu et al. have prepared G-wrapped TiO$_2$ hollow core-shell structures, in which titania core is composed of mutually independent exposed (001) and (101) faceted nanocrystals [40]. This photocatalytic system has been used for simultaneous oxidative degradation of Rhodamine B and reduction Cr(VI). The observed photocatalytic efficiency, compared with pure TiO$_2$ microspheres and P25 (Figure 3a), has been explained by Z-scheme mechanism (2nd generation Z-scheme), in which rGO acts as solid-state electron mediator, as shown in Figure 3b. Under irradiation, electrons are photoexcited from valence bands (VBs) of faceted titania nanocrystals ((001) and (101)) to their individual conduction bands (CBs). Then, rGO provides pathways for the photogenerated electrons from CB of (101) facets (possessing less positive potential) to VB of (001) facets (possessing less negative potential), and thus resulting in efficient separation of charge carriers with better redox properties, i.e., electrons in CB of (001) and holes in VB of (101) facets [40].

(**a**)

(**b**)
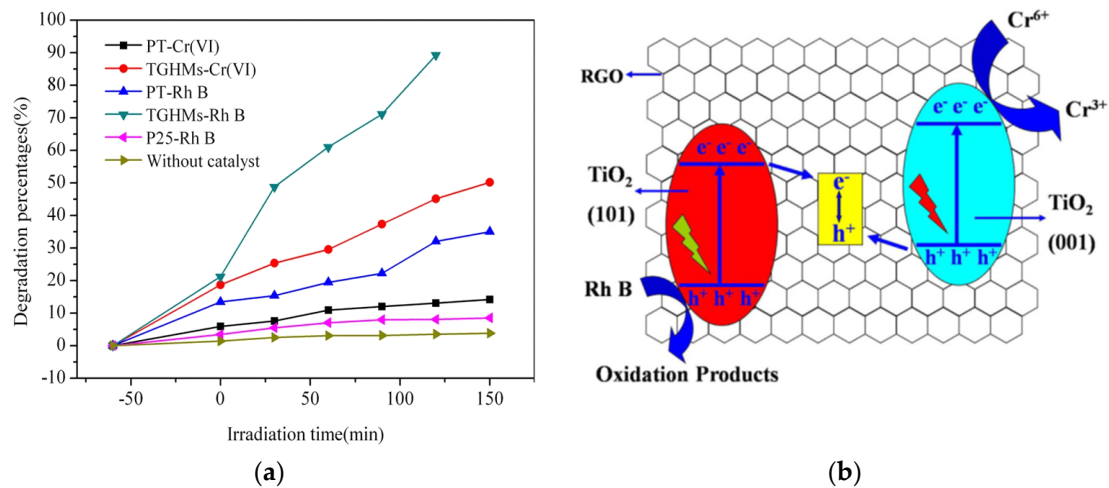
Figure 3. (**a**) Photocatalytic conversion of Cr(VI) and Rh B in single system: TGHMs–graphene-wrapped TiO_2 hollow core-shell microspheres, PT–pure TiO_2 microspheres; (**b**) Schematic graph of proposed mechanism of synergistic removal of Cr(VI) and Rh B in a Z-scheme photocatalytic system consisting of rGO and titania nanocrystals with exposed (001) and (101) facets under stimulated solar light irradiation. Reprinted with permission from [40]. Copyright 2016 Creative Commons Attribution.

The research approaches on coupling of graphene with faceted particles have not been limited to faceted titania, but also other metal oxides, such as polyhedral Cu_2O and $BiVO_4$, have been investigated. For example, Wei have obtained a ternary rGO-wrapped octahedral Ag-Cu_2O (Ag-Cu_2O/rGO) photocatalyst [41]. In the proposed novel heterostructure, Cu_2O octahedra are decorated with dense silver NPs, and wrapped with thin rGO nanosheets (Figures 4 and 5). It has been proposed that both Ag and rGO act as acceptor of photo-excited electrons from Cu_2O, improving the separation of electron-hole pairs, and thus decreasing their recombination possibility. Furthermore, the incorporation of rGO does not only suppress the recombination of charge carriers, but also prevents the agglomeration of Ag NPs. Moreover, Ag NPs could also enhance activity due to the surface plasmon resonance at vis range of solar spectrum (plasmonic photocatalysis). Therefore, Ag-Cu_2O/rGO photocatalyst has shown high photocatalytic activity and stability during photodegradation of phenol under vis irradiation [41].
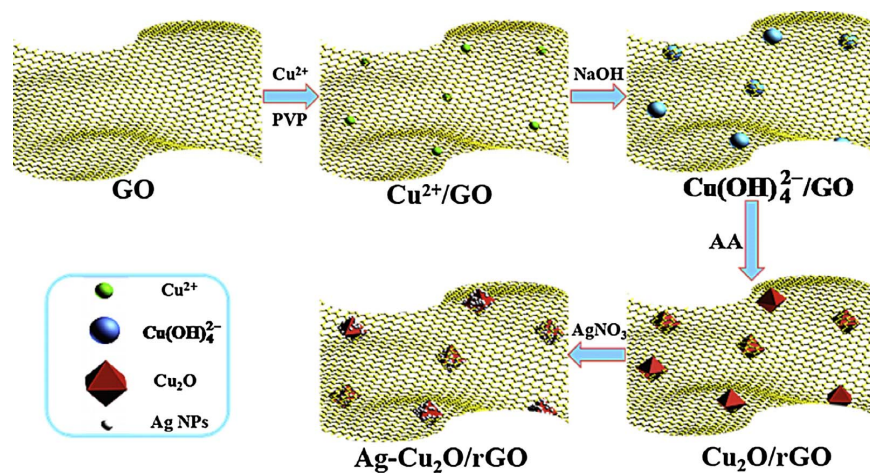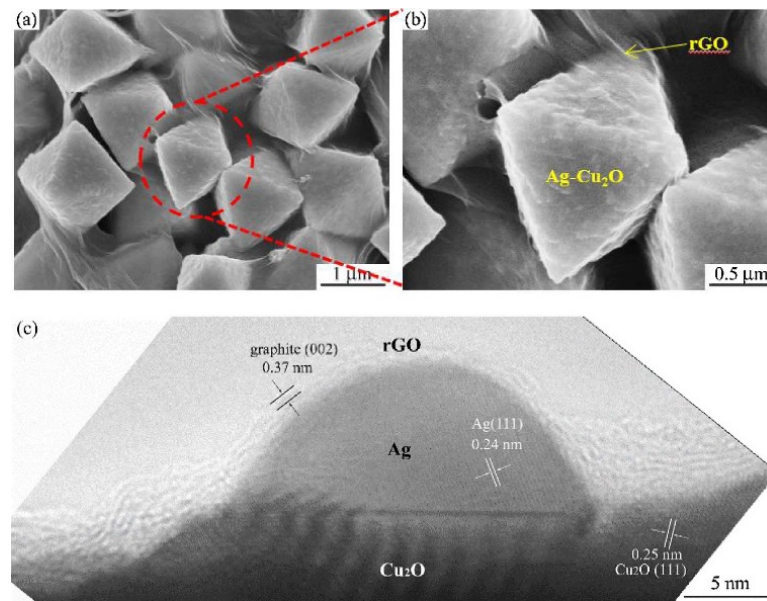

Figure 4. Schematic illustration of synthesis and structure of the Ag-Cu_2O/rGO composite. Reprinted with permission from [41]. Copyright 2018 Elsevier.

Figure 5. Microscopic images: (**a**,**b**) SEM, and (**c**) high resolution TEM of the Ag-Cu$_2$O/rGO composite. Reprinted with permission from [41]. Copyright 2018 Elsevier.

In the research focusing on BiVO$_4$, Wang et al. have presented rGO/BiVO$_4$ composites with maximized interfacial coupling by completely covering of BiVO$_4$ polyhedrons with rGO sheets by an evaporation-induced self-assembly process. In rGO/BiVO$_4$ composites, BiVO$_4$ polyhedrons have a well-defined truncated bipyramid morphology with (040) facets exposed, and rGO layers conformally covering polyhedron surfaces to form well-defined rGO/BiVO$_4$ composite (Figures 6 and 7) [42]. The as-prepared rGO/BiVO$_4$ photocatalyst has shown obviously enhanced efficiency of charge separation and improved ability of surface adsorption, resulting in significantly higher photocatalytic activity.
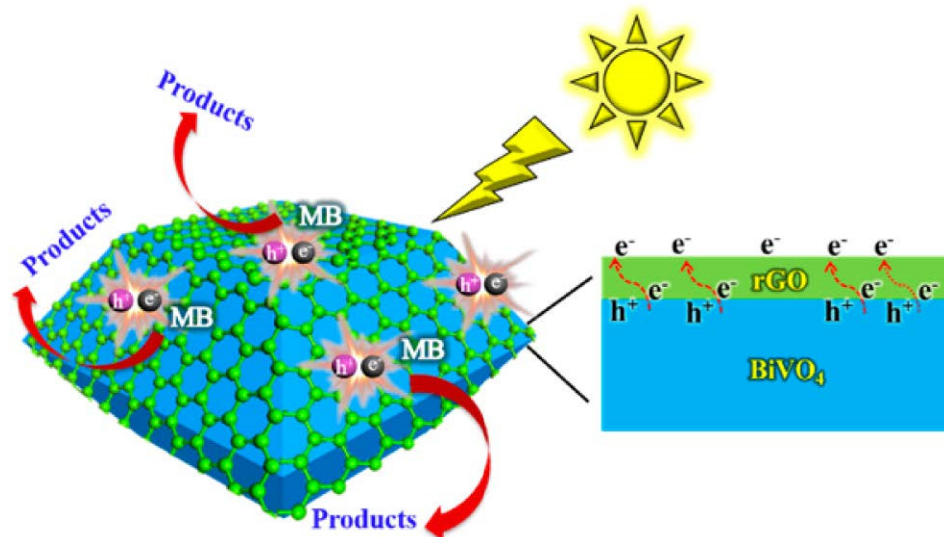
Figure 6. Schematic illustration of rGO/BiVO$_4$ with a thin rGO sheet (<5 nm) conformally covering BiVO$_4$ polyhedron, forming a well-defined interface for enhanced charge separation efficiency. Reprinted with permission from [42]. Copyright (2014) ACS.
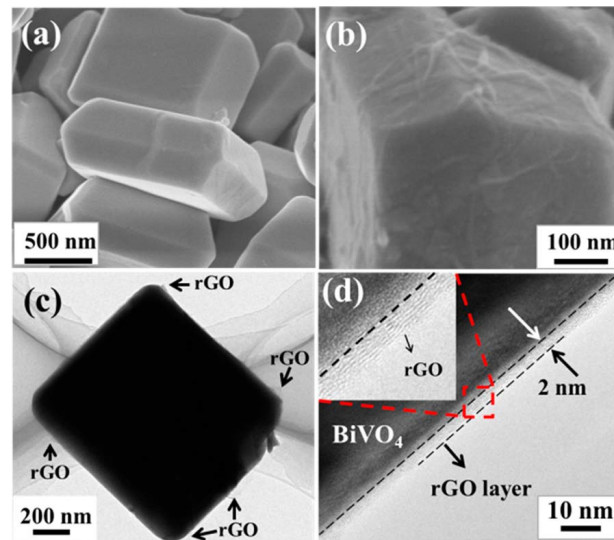
Figure 7. SEM images of as-synthesized samples: (**a**) $BiVO_4$ with smooth surface; (**b**) $rGO/BiVO_4$ with rGO layer uniformly attached on $BiVO_4$ forming a wrinkled surface, and (**c**,**d**) TEM images of $rGO/BiVO_4$ exhibiting a tight contact between $BiVO_4$ and the rGO layer (about 2 nm). Reprinted with permission from [42]. Copyright (2014) ACS.

2.2. Titania-Graphene Composites (Not Faceted Titania)

In addition to faceted titania particles, other titania samples with different morphologies have been widely studied for modification with G/rGO/CO, such as nanotubes, nanowires, nanofilms, etc. For example, Wang et al. have prepared photoelectrode composed of titania nanotube arrays (NTAs) modified with ultra-thin G nanosheet (rGO/TiO_2), as shown in Figure 8. It has been found that the hybridization of ultra-thin rGO nanosheets has resulted in negative shift of the flat band potential of titania, improving efficiency of charge separation and causing the superior photoelectrocatalytic (PEC) performance [25]. Additionally, it has been shown that much higher degradation efficiency of phenol is achieved on rGO/TiO_2 photoelectrode than that by photocatalytic (PC) and electrocatalytic (EC) processes, suggesting that photoelectric synergy effect is obtained over rGO/TiO_2 photoelectrode [43].
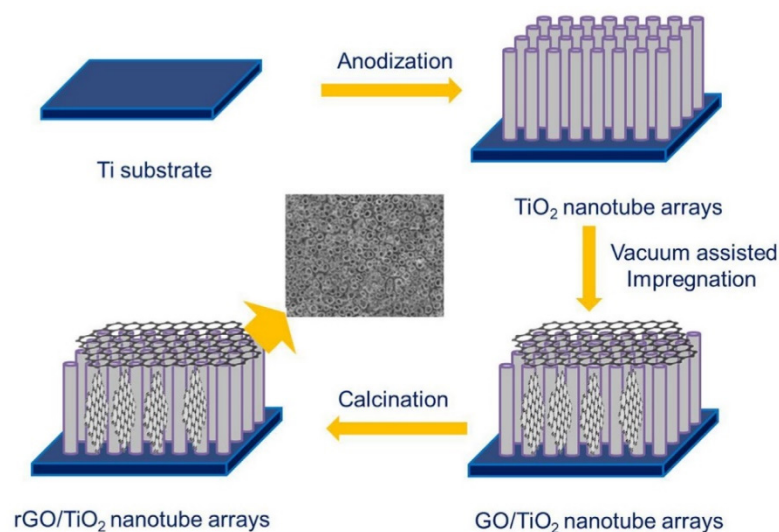
Figure 8. Scheme for the fabrication of rGO/TiO_2 photoelectrode. Reprinted with permission from [43]. Copyright 2020 Elsevier.

Pan et al. have employed the hydrothermal method to synthesize titania nanowires (NW), and then fabricate G/TiO_2 nanowire nanocomposite (GNW) [44]. The reference samples, i.e., graphene-titania nanoparticles (NP) and nanocomposite (GNP), have also been prepared for comparative study on the resultant properties and photocatalytic performance of obtained photocatalysts. It has been found that by graphene incorporation, GNP and GNW have better performance than their counterparts. Additionally, uniform dispersion of titania on graphene is critical for the photocatalytic effect of the composite (Figure 9). More importantly, it has been shown that NWs, in comparison with NPs, have more uniform dispersion on graphene with less agglomeration, resulting in better direct contact between titania and graphene, and hence further improvement in charge carriers' separation and transportation. The adsorption ability of GNW is also higher than that of GNP. It has been found that the relative photocatalytic activity of GNW is much higher than that of GNP, and pure NWs and NPs photocatalysts.
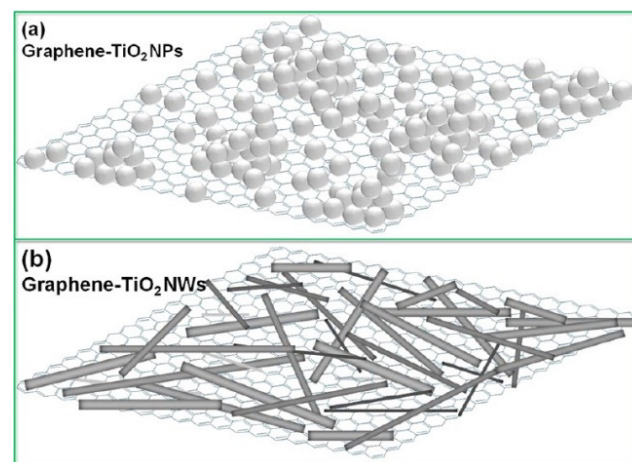
Figure 9. Schematic drawings of: (**a**) titania NPs aggregated on graphene; (**b**) titania nanowires dispersed uniformly on graphene. Reprinted with permission from [44]. Copyright (2012) ACS.

Another morphological form of titania has been used by Wang et al., i.e., mesoporous titania (m-TiO_2) as a shell of sandwich-structured r-GO/AuNP/m-TiO_2 hollow hybrids [45]. The photocatalyst, prepared by the combination of sol-gel and self-assembly methods (Figure 10), exhibits large surface area and superior adsorption ability. It has been proposed that high photocatalytic performance is attributed to the porous nature of the hybrid shells, enhanced charge separation and visible-light absorption by r-GO and AuNPs, and thus indicating that the introduction of r-GO and AuNPs improves the photocatalytic activity of titania.
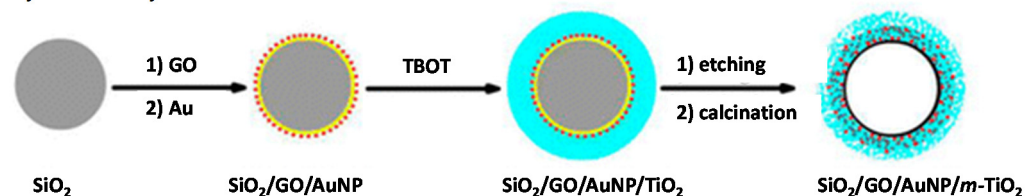
Figure 10. Schematic illustration of the synthesis steps for r-GO/AuNP/m-TiO_2 sandwich-like hollow spheres. Reprinted with permission from [45]. Copyright (2015) ACS.

2.3. Graphene-Based Photonic Crystals

Photonic crystals (PCs) are periodic optical nanostructures with unique characteristics that affect the propagation of photons, resulting in efficient light harvesting of solar radiation (UV, vis and IR). The most important property of PCs is the formation of photonic bandgap (PBG), at which electromagnetic waves are strictly forbidden to propagate at

certain frequencies, resulting from the periodicity of refractive index (n) within the materials [46]. Consequently, the effect of slow photons (reduction of photons' group velocity) is observed at both shorter and longer edges of PBG wavelengths due to the multiple scattering of photons within the nanostructure.

In recent years, the composites of PCs with graphene-based materials (G, GO, rGO) have been explored for numerous applications, such as switch [47], electronic and optoelectronic devices [48–51], sensors [52,53], surface-enhanced Raman scattering (SERS) [54], and photocatalysis [47,55,56], as exemplary shown in Table 1.

Various nanostructures of graphene-based PCs have been designed and fabricated, including one-dimensional (1D), e.g., graphene nanolayers stacked and embedded between dielectric materials [57], two-dimensional (2D), e.g., nanocavities [58], periodic cylindrical holes in multilayered graphene [30], and three-dimensional (3D), e.g., inverse opal PCs (IO-PCs). According to various theoretical models that have been reported, PBG positions could be varied according to the thickness of dielectric layer [59] and by altering the chemical potential of graphene [9,30] for both 1D and 2D graphene-based PCs.

Usually, 1D-PC structures consist of layers made from material with high-refractive index arranged periodically over the 1D structure of material with lower refractive index. The 1D PCs are commonly utilized in biosensing for biomolecular detections due to their distinct changes in resonance behavior once the binding/interaction between the target compound and PC occurs [60,61]. Graphene-based 1D PC has been identified as a good biosensor candidate due to its strong interaction with light, as proved by a theoretical study conducted by Sreekanth et al., where about 14-fold higher sensitivity has been obtained for graphene-based PC than that for SPR-based biosensor [53] since the latter might lose the sensitivity due to damping in optical waves [62].

In recent theoretical study by Pourmahmoud and Rezaei, it has been revealed that dielectric coupled with layers of graphene shows additional stopband apart from Bragg's PBG, known as "graphene PBG" [51]. Interestingly, the changes in incident angle of irradiation of the 1D PC do not exhibit significant differences in the PBG width, which is in contrast to any 3D inverse opal (IO) PC, where the stop band position varies in dependence on the angle of incident light [63,64]. However, in contradiction to studies by Pourmahmoud and Rezaei, it has been shown that graphene layer deposited on SiO_2 1D PC exhibits an enhanced absorption [65].

Table 1. Graphene-modified PCs: preparation, properties and performance.

PCs	Loading Method	Applications	Findings	Ref.
(GQD)-TiO_2 film	TiO_2 immersion in GQD suspension	SA degradation; $\lambda > 400$ nm	enhanced activity	[55]
α-Fe_2O_3/graphene	spin coating and thermal treatment	ICPE measurement; Xe lamp	2.6-fold higher than reference	[66]
graphene	-	optical absorption	enhanced abs.	[49]
graphene PC fiber	-	optoelectronics	stronger broadband response	[50]
α-Fe_2O_3/GIO	carburization; nickel oxide IO and CVD	PEC water splitting	1.4-fold higher photocurrent den.	[67]
rGO/Pt/3DOM TiO_2	immersion and calcination to form r-GO	MO degradation; $\lambda > 420$ nm;	4-fold increase	[68]
TiO_2@ rGO@Au	immersion and calcination	PEC water splitting; 300-W Xe lamp	2-fold enhancement	[69]
IO-SnO_2/G microspheres	immersion and calcination	MO degradation 300-W Hg lamp; $\lambda = 365$ nm	enhanced activity	[70]

Table 1. *Cont.*

PCs	Loading Method	Applications	Findings	Ref.
graphene	-	biosensor	14.8 times higher sensitivity *	[53]
GO/TiO$_2$ IO	immersion in GO nanocolloid	MB degradation 150-W Xe lamp with 305 nm and 400 nm cut off filter	enhanced activity	[71]
GO/TiO$_2$ IO film	immersion in GO nanocolloid	SERS detection	lower LOD	[54]
rGO/TiO$_2$	immersion and calcination	MB and SA degradation 150-W Xe lamp with 305 nm and 400 nm cut off filter	improved photodegradation	[56]
NPS-IOC	-	organic pollutants adsorbents	excellent adsorption	[72]

α-Fe$_2$O$_3$/GIO—coupling α-Fe$_2$O$_3$ with a 3D graphene inverse opal; abs.—absorption; CVD—chemical vapor deposition; den. —density; ICPE—incident photon-to-current efficiency; LOD—limit of detection; MB—methylene blue; MO—methyl orange; NPS-IOC—3D nitrogen, phosphorus, and sulphur co-doped graphene-like carbon nanosphere with IO structure; PEC—photoelectrochemical; rGO/Pt/3DOM TiO$_2$—three dimensionally ordered macroporous TiO$_2$ with platinum (Pt) and reduced graphene oxide (rGO); SA—salicylic acid; SERS—surface-enhanced Raman scattering; * sensitivity in comparison with SPR based biosensor.

For 2D structures, an interesting theoretical study has been performed on graphene/silver (with surface plasmon resonance, SPR) coated PC fiber, where graphene deposition has been identified as the promising method to prevent the oxidation of silver that might weaken the SPR effect for the sensor efficacy [52]. It is well known that though graphene has broad light absorption range in electromagnetic wave spectrum, the total optical absorption is still weak and requires some aid for enhancement, e.g., from supporting materials. In this sense, the coupling of graphene with PCs might significantly improve the ability of optical absorption, as already reported [50]. Accordingly, introduction of single layer of graphene into 2D PC (nanocavity) has been postulated to enhance the light-matter interaction, as confirmed by a model study carried out by Gan et al. [58].

Controlled engineering that involves the design of IO heterostructures (3D), such as the coupling of conductor, semiconductor [67] and plasmonic nanomaterials [48,73], has gained attention and been considered as an efficient method to enhance the performances of various materials, including graphene-based IO PCs, where graphene acts either as the backbone material of PCs or co-catalyst to improve the conductivity of the overall coupled PC-based materials.

The fabrications of graphene-based PCs, where graphene-like materials (GO/rGO) act as co-catalysts, has been mostly carried out by immersing/dipping the IO PC into GO colloidal suspension with subsequent post-thermal treatment (calcination) [55,68,69,71]. On the other hand, the formation of graphene-like materials as the backbone material of IO PC requires at least three-step procedure i.e., (i) preparation of template (opal), (ii) infiltration of opal with targeted material, and (iii) the removal of sacrificial template. For example, the opal template has been infiltrated with precursors of dopants (N, P, S) along with carbon (to form carbonaceous IO), and then pyrolyzed under inert conditions in order to form multi-heteroatom-doped graphene-like carbon nanospheres IO PC [72]. It has been shown that high temperature (700–1000 °C) is necessary for carbonization and carburization to fabricate graphene as the IO PC backbone material [67,74].

The role of graphene as IO PC material has been identified by Yoon et al., and some problems, e.g., charge carriers' recombination and slow electrons' pathway in α-Fe$_2$O$_3$, have been overcome by utilizing the advantage of PC via trapping of photons, and improving the charge carriers' mobility via organized network [67].

A novel ternary IO PC photocatalyst has been developed by Hua et al., consisting of rGO, platinum (as co-catalyst) and titania as the backbone material [68]. It has been proposed that rGO improves the charge carrier's separation apart from enhanced light harvesting, as illustrated in Figure 11. Similarly, Bopella et al. have postulated that the excellent carriers' transport (extended lifetime of electrons) by rGO in ternary photocatalyst (rGO/Au/TiO$_2$) and the synergistic effect between Au NP (SPR effect) and rGO for light harvesting are responsible for the amplified incident photon-to-electron conversion efficiency in the photoelectrochemical (PEC) study [69]. Diamantopoulou et al. have further confirmed the enhanced charge carriers' separation by rGO-functionalized on TiO$_2$ IO PC with the highest rate of salicylic acid photodegradation and the lowest photoluminescence intensity, as compared to GO-TiO$_2$ IO (without thermal treatment) and pristine PC, as shown in Figure 12 [56].

(a)

(b)
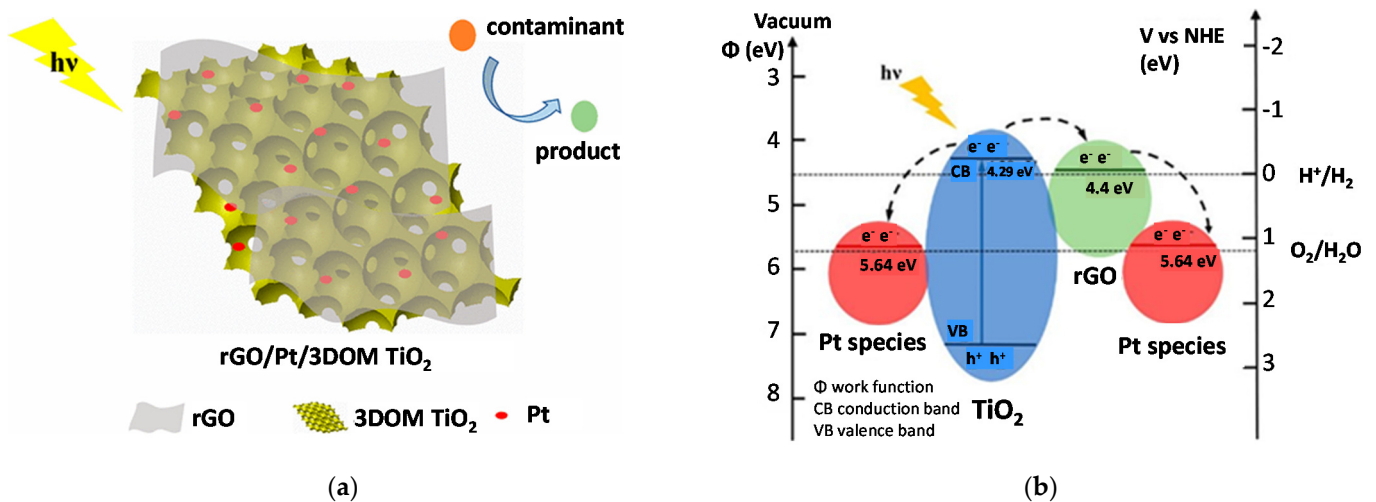
Figure 11. Schematic illustrations of: (**a**) the morphology of TiO$_2$ IO co-modified with Pt NPs and reduced graphene oxide (r-GO), and (**b**) the proposed charge carriers' separation and migration in rGO/Pt/TiO$_2$ (not plasmonic activation), rGO-green, Pt-red, TiO$_2$-blue; Reprinted with permission from [68]. Copyright (2019) ACS.

(a)

(b)
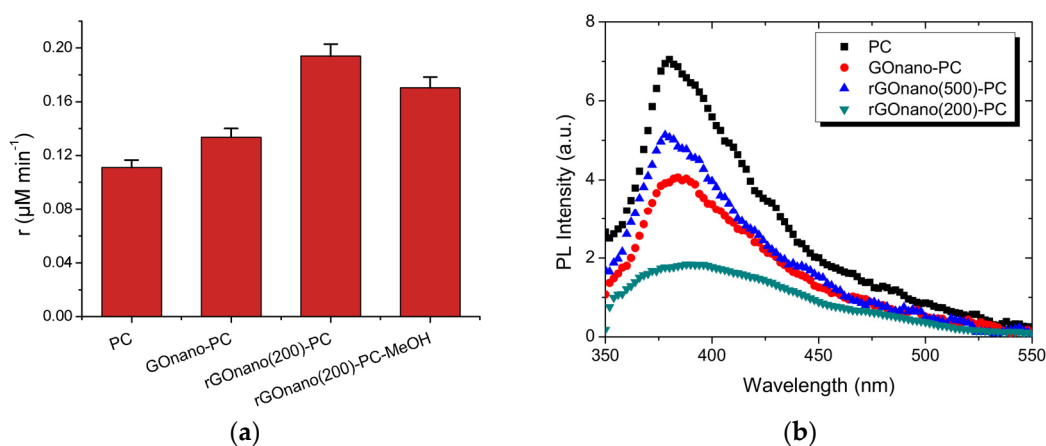
Figure 12. (**a**) Photocatalytic reaction rate of salicylic acid degradation and (**b**) photoluminescence spectra of pristine TiO$_2$ PC, GOnano-PC and rGOnano functionalized on TiO$_2$ PC. Reprinted with permission from [56]. Copyright (2013) Creative Commons Attribution.

One of the prerequisite aspects in the case of G/rGO-modified PCs is the loading amount of G/rGO, which is critical for the enhancement of photocatalytic activity, and thus an optimum amount of G/rGO loaded on PC results in the best performance. For example, the highest photodegradation of methyl orange has been achieved in the presence

of photocatalyst containing 0.06 wt% rGO incorporated into SnO_2 IO, as compared to bare and modified SnO_2 IO containing larger content of rGO (0.15 and 0.82 wt%) [70]. This observation is valid for any materials/compounds loaded/deposited on the surface of PCs, e.g., noble metals, indicating the importance of optimum content of modifiers, since lower/higher content diminishes significantly the photocatalytic performances, due to various reasons, e.g., "screening effect" [75,76].

In summary, the coupling of photonic effect (PBG from PCs) and conductivity as well as light harvesting ability (from graphene-like materials) might result in high improvement of efficiency and performance of advanced materials in various fields, due to the combination of enhanced optical path length and improvement of charge carrier's separation.

3. Environmental Applications of Graphene-Based Photocatalysts

3.1. Antimicrobial Properties of Graphene-Based Composite Photocatalysts

Various antimicrobial materials have been intensively studied to protect humans, animals, and the whole environment, including metals (e.g., silver and copper) [77–79], titania [80–84] and organic compounds (e.g., antibiotics and chlorine compounds). Although many of them have been widely applied to daily necessities, the concerns about environmental contamination, the possible toxicity [85], antibiotic resistant bacteria (ARB), and high costs still remain. From these points of view, carbon (graphene) compounds might be the promising antimicrobial materials.

It should be pointed out that the study on the antimicrobial activity of graphene species is a new topic as first report on GO/TiO_2 was published by Akhavan and Ghaderi in 2009 [86]. In this report, though GO/TiO_2 composites have exhibited much higher activity than titania, GO seems to be inactive both under UV-vis irradiation and in dark condition and, thus, it can only accelerate the activity of titania. In 2010, the same authors have proposed that graphene nanosheets in the form of nano-walls have shown bactericidal activity both for gram-negative (*Escherichia coli*) and Gram-positive (*Staphylococcus aureus*) bacteria (several percent to several tens of percent survival) with RNA effluxes, and rGO has higher activity than GO [87]. Since then, many studies have been performed and even summarized in some review papers and, thus, in this section, only the recent reports are presented (summarized in Table 2) and discussed.

Table 2. Graphene compounds for microbial disinfection.

Sample	Preparation Method	Experimental Conditions	Findings	Ref.
GO G	HM (GO)/ GO red. by *Allium cepa* extract (G)	PA; *Streptococcus* sp., *Staphylococcus* sp., *E. coli* or *P. aeruginosa.*	activity: GO > G	[88]
GO	sonication of commercial GO to reduce sample polydispersity	CC; *E. coli* or *S. aureus*	low conc.: enh. growth; high conc.: inh. growth.	[89]
GO rGO	graphite oxidation by BaM (GO) and BrM (rGO)	CC; *E. coli* cultured in LB or NB media	in LB 35% and 45% CFU red.; in NB 80% and 85% CFU red. for GO and rGO, respectively (24 h)	[90]
rGO	graphite oxidation by $KMnO_4$ (GO); GO red. by L-ascorbic acid (rGO)	Fluorescence analysis using GFP-labelled *E. coli*	in NaCl no effect; in NB inh. growth (nutrient ads.)	[91]
CS@GO	HM (GO); GO and CSCl mixing, evaporating, freeze-drying (CS@GO).	CC; *E. coli* or *S. aureus*	96% inhibition for 0.6% GO; stable after 3 times (>90%)	[92]

ads.—adsorption; BaM—Bangal method; BrM—Brodie Method; CC—colony-counting method; conc. —concentration; CS—chitosan; enh.—enhanced; HM—Hummers' method; inh.—inhibited; LB—Luria-Bertani; MH—Mueller-Hinton; NB—nutrient broth; PA—photoabsorption measurements by UV/vis at 500–600 nm; red. —reduction.

For example, it has been shown that GO exhibits higher bactericidal activity than graphene (prepared by the reduction of GO by *Allium cepa* extracts), possibly due to the typical aggregation of graphene [88]. The concentration of GO significantly influences the bacterial viability, i.e., at low concentrations, GO forms floating scaffolds, which enhances bacterial growth, whereas at high concentrations, GO forms scaffolds, which inhibits the bacterial growth [89]. Moreover, it has been suggested that the morphology of GO membrane (roughness, sharpness, and curvature) is important for bactericidal effect, i.e., the rougher or sharper the membrane is, the higher is bactericidal activity [93,94].

Interestingly, it has been shown that culture media influence the bactericidal effect [90,91]. For example, bacteria are inactivated on GO and rGO (ca. 45 and 35% inhibition at 24 h for GO and rGO, respectively) in Luria–Bertani (LB) medium due to oxidative stress (the deficiency of Mg^{2+} and Ca^{2+} ions), but antibacterial effect is negligible in Mueller–Hinton (MH) medium (with 5–10 higher concentration of Mg^{2+} and Ca^{2+} ions) [90]. Gusev et al. have proposed that rGO has no direct bacterial toxicity, i.e., rGO does not show the bactericidal activity in physiological saline solution, even though the aggregation of bacteria and rGO is observed, resulting in the efficient removal of live/dead bacteria by filtration [14]. Moreover, inhibited growth of bacteria in nutrient broth (NB) medium has not been caused by antibacterial activity of rGO, but only because of the adsorption of nutrients on rGO (no cell damages) [91].

It should be mentioned that carbon (not necessary in graphene form) could be also responsible for bactericidal activity. For example, practically same antibacterial activity has been achieved on graphene (rGO)- and carbon-modified titania samples (prepared by same method via laser synthesis) both in the dark and under vis irradiation (three times higher activity under vis than that in the dark) [11]. Interestingly, both samples show also almost the same activity for oxidative decomposition of organic compounds under UV and vis irradiation, whereas rGO/TiO$_2$ sample exhibits much higher activity only for evolution of hydrogen under UV irradiation, indicating that graphene might work as co-catalyst for hydrogen evolution.

A total of three main mechanisms of bactericidal action of graphene and its compounds have been considered, as follows: (i) the cell membrane damage [87,95], (ii) oxidative stress by reactive oxygen species (ROS) [96], and (iii) charge transfer [97]. It should be pointed out that, generally, the efficiency of antimicrobial agents for organisms is quite different not only for different categories (e.g., mammalian and bacteria), but even among the species of the same genera (e.g., *Aspergillus niger* and *A. melleus*). Indeed, Nguyen et al. have clearly shown different response for different fungi to G/GO, where G inhibits the growth of *A. flavus*, whereas *A. niger* is inhibited by GO, indicating that G and GO have different toxicity mechanisms against fungi (e.g., hyphae cell wall damage, and changes in synthesis of enzymes) [98].

Further applications of graphene materials have been examined for the microorganisms that cause chronic wounds and disease (due to prolonged inflammation, persistent microbial infections and multispecies drug-resistant microbial biofilms). For example, antimicrobial and antibiofilm properties of GO against bacterial wound pathogens, such as *S. aureus*, *Pseudomonas aeruginosa*, and yeast *Candida albicans*, have been elucidated, and it has been considered that the interactions between GO and microorganisms, i.e., hydrogen bond interactions between carbonyl and hydroxyl groups abundant in polysaccharides and GO and π-π interactions between DNA and RNA bases and graphenic domains in GO, result in the inhibition of microorganisms' aggregation and adhesion on the surfaces [99]. Interestingly, different from the direct killing of microorganisms by GO, it has been proposed that poly(ethylene glycol-amine)-derivatized GO nanosheets (PEG-GO) can stimulate and activate macrophages (M1 and M2) and more efficient phagocytosis of *C. albicans* is observed than that on unstimulated GO, indicating the possibility of avoiding some chronic infectious diseases [100].

Moreover, GO modification with organic compounds that possess the antimicrobial activity and biocompatibility have been intensively studied very recently, e.g., chitosan

(CS) [92,101–103], curcumin [104,105], antimicrobial agents (isoniazid (INH), amikacin (AMK) and linezolid (LZD), lincomycin hydrochloride (LMH), chloramphenicol (CPC) and gentamycin sulfate (GMS) [106,107]) and dyes [108]. Chitosan exhibits high biocompatibility, biodegradability and antibacterial properties [109]. The possible mechanism of the antibacterial activity is based on the assumption that the positively charged amino group in CS could interact with negatively charged components on the surface of bacterial cells [110]. Chitosan-modified GO (CS@GO) significantly inhibits the bacterial survival (ca. 96% of inhibition) with good stability during three cycles of experiments (above 90%), and importantly, CS@GO shows higher effect than reference samples, i.e., CS or GO [92]. In addition, chitosan-polyethyleneimine (PEI)-graphene oxide (GO) nanocomposite removes also the heavy metals (Cr(VI), Cu(II), and Pb(II)), nitrate and bacteriophage [103]. It has also been reported by Ramasamy et al. [108] that the alizarin (AZ), the dye known as anti-biofilm formation agent [111,112], has conjugated on GO (AZ-GO), which results in the inhibition of biofilm formation of *C. albicans*. Additionally, the treatment of *C. albicans*-infected nematode (*Caenorhabditis elegans*) with AZ-GO has caused an increase in the survival of *C. elegans*. Accordingly, the presence of GO stabilizes the conjugated antimicrobial agents and gives higher activity than agents themselves.

The nanohybrids of graphene with metals and metal oxides have also been proposed in order to obtain the efficient antimicrobial agents, e.g., Ag [113–117], Ti [118], NiO [119], ZnO [120–123] and TiO_2 [124–126], as summarized in Table 3.

**Table 3.** Graphene-based composites with metals and metal oxides for microbial disinfection.

Sample	Preparation Method	Experimental Conditions	Findings	Ref.
GO-Ag	$AgNO_3$ aq. added to GO under constant stirring	DD; *E. coli* or *S. aureus*	conc. dependent inhibition zone; *E. coli* > *S. aureus*	[113]
GO Ag-GO	HM (GO); GO, PVP, α-D-glucose, Ag/NH_3 at 45 °C.	EEAA, NR, LDH, ROS; AMNRLW	Ag-GO > GO, dec. EEAA/NR, LDH release and ROS generation	[115]
AgNPs/TETA-GO	HM (GO)/ self-assembly using TETA as a bridging agent	CC; *E. coli* or *S. aureus*	MIC: 0.125 mg/mL (*E. coli*), 0.25 mg/mL (*S. aureus*)	[127]
PVA/AgNPs-GO	HM (GO)/ Ag^+ red. on PVA-GO by L-ascorbic acid	EUCAST; *E. coli* or *S. aureus*	2 wt% Ag—4 log red. *E. coli*/*S. aureus* (24 h)	[128]
GO/CS/TiO_2	HM (GO)/ GO dropwise into CS, TiO_2 addition	DD, L/D; *B. subtilis* and *A. niger*	inh. colony formation; most active GO:CS:TiO_2 = 1:20:4	[129]
Cu_2O-TiO_2/rGO	USR followed by WI	DD and MIC; *S. aureus*, *E. coli*, *S. oralis*, *Pseudomonas aeruginosa* under vis	bactericidal activity: *S. aureus* > *P. aeruginosa* ≈ *E. coli* > *S. oralis*.	[124]

AMNRLW—Aquatic microorganisms in natural river/lake water; CC—colony-counting method; conc. —concentration; CS—chitosan; DD—disc diffusion method; dec. —decreased; EEAA—extracellular enzyme activity assay; enh.—enhanced; EUCAST—EUCAST dilution method; HM—Hummers' method; inh.—inhibited; L/D—live/dead fluorescence assay; LDH—lactate dehydrogenase; MIC—minimum inhibitory concentration; NR—nitrification rate; red.—reduction; ROS—reactive oxygen species, USR—ultrasonic reduction WI—wet impregnation.

Silver deposition on GO/rGO significantly enhances the antimicrobial activity (against *E. coli*, *S. aureus*, oral pathogens *C. albicans*, *Lactobacillus acidophilus*, *Streptococcus mutans*, and *Aggregatibacter actinomycetemcomitans*) due to the intrinsic activity of silver [113–117]. The effects for aquatic microbial communities have been studied by Ko et al. [115], and it has been proposed that both GO and Ag-GO decrease the activity of extracellular enzymes and generate ROS, e.g., singlet oxygen, hydroxyl radicals (•OH), super oxide anion rad-

icals ($^\bullet O_2{}^-$) and hydrogen peroxide (H_2O_2). It should be pointed out that though ROS are detected only at the beginning stage for GO due to its further aggregation, Ag-GO generates ROS continuously for 48 h, indicating that Ag-GO has high stability in natural water. Luo et al. have shown that uniformly deposited Ag NPs on triethylenetetramine (TETA)-functionalized GO (TGO) show significant antimicrobial efficiency for both gram-positive and gram-negative bacteria with higher efficiency against the latter [127]. Similarly, poly(vinyl alcohol)/Ag NPs-GO (PVA/AgNPs-GO) nanocomposite, fabricated through one-step environmentally friendly chemical reduction method, shows bactericidal activity towards both *E. coli* and *S. aureus*, for 2 wt% of Ag, but the composite with lower content of silver is inactive [128]. Therefore, it has been proposed that GO stabilized metallic deposits and organic compounds.

In addition to metal NPs, semiconductor photocatalysts, e.g., TiO_2 [124–126], ZnO [120–123] and NiO [119], have also been used for graphene modifications, as shown in Table 3. Many studies have revealed that G/rGO/GO as a support for the photocatalysts could enhance the charge transport (as also discussed in previous sections), resulting in improved photocatalytic activity. Xu et al. have demonstrated that $GO/CS/TiO_2$ composite exhibits significant suppression of colony-forming against bacteria *Bacillus subtilis* and filamentous fungi *Aspergillus niger* biofilm formation, despite the material does not show the cytotoxicity against mammalian and plant cells (Figure 13) [129]. The disinfection properties of GO and GO-based composite photocatalyst might be also enhanced by the modification with metals. For example, copper, one of the most efficient metals against microorganisms, has been introduced into semiconductor/GO in order to obtain enhanced activity in the dark and vis absorption. Jiang et al. have revealed that when Cu/ZnO@rGO reacts with bacterial cells, the composite induces the electron donor on the cell surface to react with oxygen molecules to generate and accumulate $^\bullet O_2{}^-$, causing the oxidative stress (e.g., membrane damage and protein leakage), as shown in Figure 14 [123]. The modification of titania with rGO improves the photocatalytic efficiency due to enhanced charge separation, hindered charge carriers' recombination and vis absorbance (due to the mid-gap states above the valence band of titania) [130,131]. Interestingly, Cruz-Ortiz et al. have revealed the dominant ROS formed on TiO_2-rGO for the bactericidal effect, i.e., H_2O_2, $^\bullet OH$, and singlet oxygen under UV-vis, and only singlet oxygen under vis [126]. Moreover, Cu_2O-TiO_2/rGO exhibits higher antibacterial activity than bare TiO_2 under vis irradiation, i.e., larger zone of inhibition and lower MIC for both Gram-positive and Gram-negative bacteria [45], which is not surprising as titania is usually inactive under vis irradiation. Whitehead et al. have compared the antimicrobial activity of graphite, GO, ZnO-GO and Ag-GO against *E. coli*, *S. aureus*, *Enterococcus faecium* and *Klebsiella pneumoniae*, and it has been found that though the antimicrobial effect (determined as MIC) does not depend on the bacteria group (gram-positive/negative), but is related to the microorganisms' physiology [132]. Interesting study has been shown by Pulingam et al. indicating that the mechanism of action is influenced by the degree of contact between GO and bacterial cells [133]. The species of bacteria aggregated into pairs or present as single cells (e.g., Gram-negative *E. coli*) are more sensitive due to larger exposure to GO, whereas bacteria existed as clusters (e.g., gram-positive *S. aureus*) are more resistant due to the benefits from corporate life, which means that only outer bacteria are exposed (screening effect).
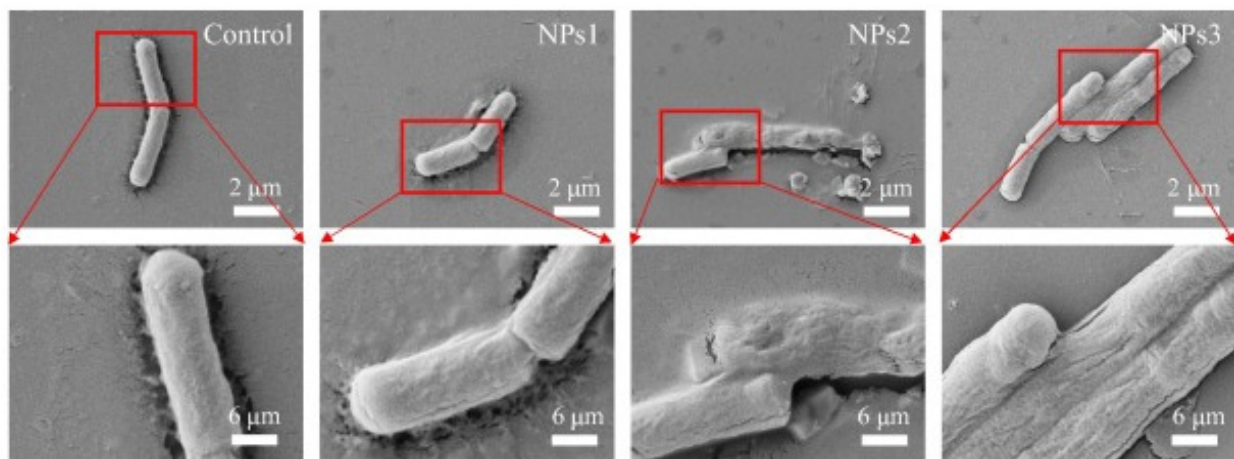
Figure 13. SEM images of *B. subtilis* cells without treatment and treated with 10 mg/mL GO@CS@TiO$_2$ for 2 h. NPs1, NPs2 and NPs3 indicates the ratio of GO/CS/TiO$_2$ equals to 1:20:2, 1:20:4 (the best activity), 1:20:8, respectively. Reprinted with permission from [129]. Copyright (2017) Elsevier.
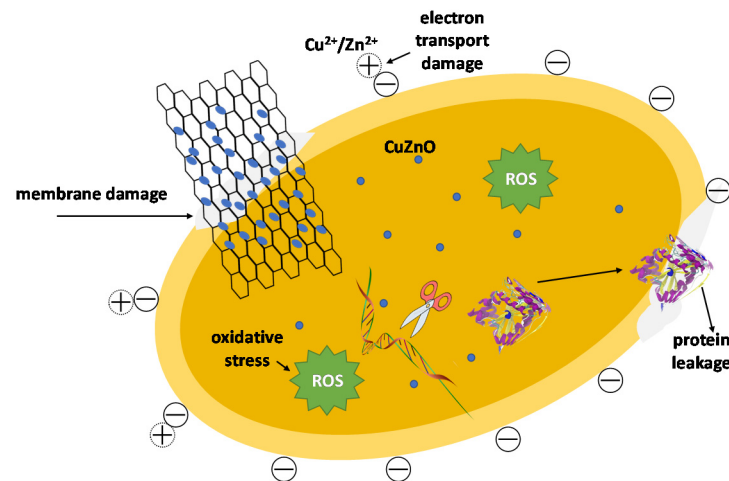
Figure 14. Antibacterial mechanism of CuZnO@RGO nanocomposites, drawn based on reference [123].

Recently, interesting application of graphene has also been shown, i.e., the laser-induced graphene (LIG) filter, a microporous conductive graphene foam, formed by direct photothermal conversion of a carbon precursor by a commercial CO$_2$ laser cutter [134]. It has been shown that bacteria are captured and destroyed efficiently by Joule-heating, reaching ca. 380 °C when a potential is applied.

Graphene derivates, have also been proposed as antiviral materials to fight against pseudorabies virus (PRV), porcine epidemic diarrhea virus (PEDV), Herpes simplex virus type 1 (HSV-1), influenza A virus (H9N2) or SARS-CoV-2 [135]. Blocking of the virus binding sites with the graphene to prevent them from entering the target cells is the main mechanism. It has been demonstrated that negatively charged and sharp-edged GO causes the single-layer viral capsid damage by direct contact. High hopes are related to the use of graphene and its composites, e.g., with metals and polymers, for development of electrochemical, piezoelctric and Cluster Regulatory Interspaced Short Polindromic Repeats CRISPR/Cas technology-based biosensors for sensitive, early and fast diagnosis of virus infections.
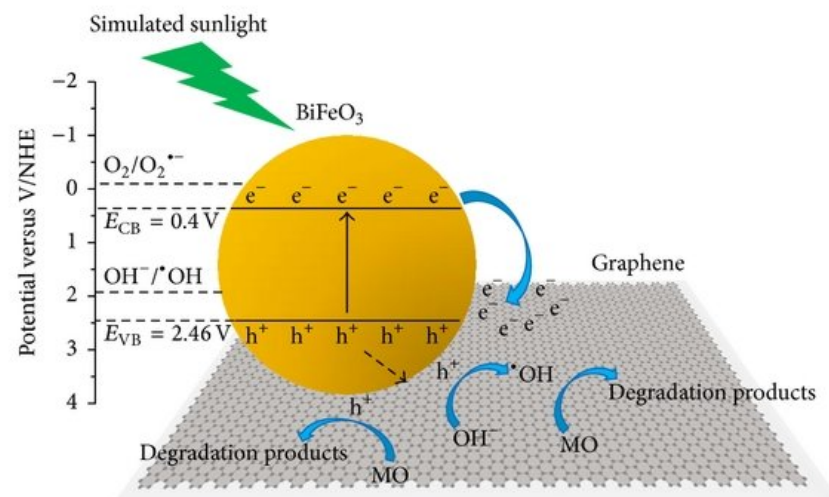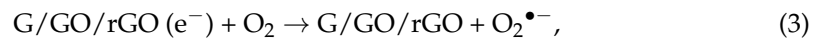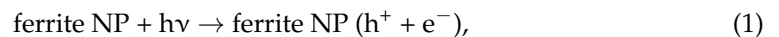
In summary, G/rGO/GO might work as efficient antimicrobial agents, especially when coupled with other antimicrobial agents, e.g., antimicrobial organic compounds, metal nanoparticles and photocatalysts. Many applications of antibacterial properties of graphene-based derivates have already been demonstrated, including bandage, gauze and

slices, paper for food packaging, face mask, filters for purifying water or next generation biocomposites for dental and bone implants. Therefore, it is expected that G/GO/rGO-based materials will be available for broad application soon.

3.2. Magnetically Separable Graphene-Based Composite Photocatalysts

In recent years, the composites of graphene with magnetic particles have been intensively studied for various applications, including biomedical purposes (controlled-release drug delivery [136], nano-supports [137], protein and peptides extraction [138], biosensing [139], etc.) and environmental purification (heavy metal removal [140], inorganic and organic contaminants sorption [141,142]). Graphene, due to good electron conductivity, high adsorption capacity and extremely high specific surface area [143], is also widely used as photocatalytic material. The coupling of graphene with ferromagnets allows the formation of effective material for organic recalcitrant photodegradation.
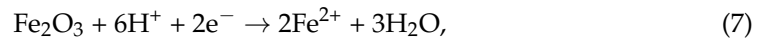
Magnetic NPs in photocatalysis could perform a dual function, i.e., as (i) a semiconductor in heterojunction, and (ii) a material applied for post-process photocatalyst separation. In most cases, nanoferrites are used as photocatalytically active materials since efficient separation of photogenerated charge carriers is related to synergistic effect between two semiconductors [144]. Ferrites, as semiconductors with narrow bandgap, e.g., $CuFe_2O_4$—1.42 eV [145], $AgFeO_2$—1.9 eV [146], $ZnFe_2O_4$—1.68 eV [147], Fe_3O_4—0.1 eV [148], could be easier photoexcited with sunlight than graphene. Consequently, photogenerated electrons are transferred to graphene sheets, where they take part in formation of ROS, and thus causing the degradation of organic pollutants. General chemical reactions (Equations (1)–(5)) as well as schematic mechanism of organic compounds' degradation on G/BiFeO$_3$ (Figure 15) are shown below [149].

$$\text{ferrite NP} + h\nu \rightarrow \text{ferrite NP } (h^+ + e^-), \tag{1}$$

$$\text{ferrite NP } (e^-) + \text{G/GO/rGO} \rightarrow \text{ferrite NP} + \text{G/GO/rGO } (e^-), \tag{2}$$

$$\text{G/GO/rGO } (e^-) + O_2 \rightarrow \text{G/GO/rGO} + O_2^{\bullet-}, \tag{3}$$

$$\text{ferrite NP } (h^+) + OH^- \rightarrow \text{ferrite NP} + {}^{\bullet}OH, \tag{4}$$

$$\text{organic pollutant} + O_2^{\bullet-} + {}^{\bullet}OH \rightarrow \text{degradation products}, \tag{5}$$

Figure 15. Schematic mechanism of photodegradation of organic pollutants on BiFeO$_3$-graphene heterojunction. Reprinted with permission from [149]. Copyright (2013) Creative Commons Attribution.

Nonetheless, especially in acidic conditions, direct ferromagnet-semiconductor structure could not be stable due to photobleaching and oxidation-reduction of iron ions in ferromagnet NPs, caused by charge carriers side reactions (Equations (6)–(9)) [150]. As a

result, iron dissolution could cause poisoning of photocatalyst and, as a consequence, breakdown of the heterojunction structure [151].

$$Fe^{3+} (s) + e^- \rightarrow Fe^{2+} (s), \tag{6}$$

$$Fe_2O_3 + 6H^+ + 2e^- \rightarrow 2Fe^{2+} + 3H_2O, \tag{7}$$

$$Fe_3O_4 + 8H^+ + 3e^- \rightarrow 3Fe^{2+} + 4H_2O, \tag{8}$$

$$Fe^{2+} (aq) + h^+ \rightarrow Fe^{3+} (aq), \tag{9}$$

Therefore, the junction of ferrite NPs and graphene sheets is a conceivable solution for creating universal material with both photocatalytic activity and magnetic separability. As photogenerated electrons migrate only from ferrite to graphene, the leaching of ions is inhibited, and the adsorption and photocatalytic properties are increased [152,153].

In practice, ferrite-graphene hybrid photocatalysts are successfully used for degradation of organic recalcitrant chemicals, mostly dyes, e.g., methylene blue (MB) or methyl orange (MO), but also pesticides and antibiotics [154–157]. Various types of magnetic materials have been proposed for graphene-based heterojunction systems and mostly spinel ferrites with general chemical formula of MFe_2O_4, where M is Co, Ni, Mn, Fe, Zn, Bi, etc. [158]. Common use of those materials is mainly caused by simple sol-gel or hydrothermal/solvothermal synthesis methods [159–161]. The structure of spinel ferrite is based on a closed cubic oxygen lattice, in which tetrahedra and octahedra are occupied by metal cations (Figure 16). Spinel that contains only divalent ions at tetrahedral sites is called normal, whereas that with divalent ions at octahedral sites is called inverse [162].
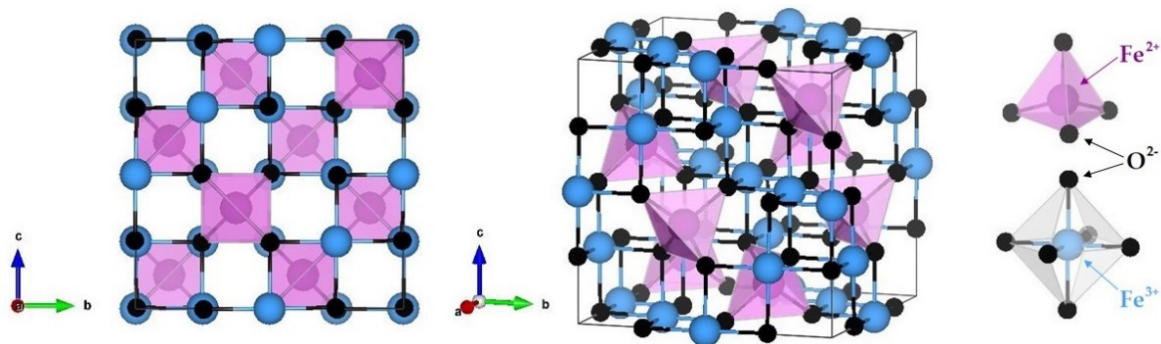

Figure 16. Spinel ferrite structure on Fe_3O_4 NP example (octahedra not marked for clearer structure visibility).

The unpaired electrons exist in most of spinel ferrites structures, which in an external magnetic field, create the partial magnetic moments, due to their ordered orbits movement around individual atoms. The created magnetic moments are equaled to the macroscopic magnetic properties of magnetic material. Moreover, the existence of the magnetic domains, i.e., areas in the material structure where partial magnetic moments are directed in one direction, is characteristic for ferromagnets [163]. In photocatalysis, magnetic separation is efficient for high saturation magnetization (Ms) values. Ms represents the force of interaction between the magnetic particle and the current magnetic field. It has been suggested that Ms value of 1 Am^2/kg is enough for efficient separation [164], but there are no many reports to support this, and thus there is disagreement between researches on this aspect. An overview of the most widespread ferromagnets-graphene heterojunction systems, together with their photocatalytic properties for degradation of organic pollutants, is summarized in Table 4.

Another important issue of graphene-based magnetic photocatalysts is their recovery after photocatalytic process and reuse in the next experiments. The aforementioned Ms parameter, determined by means of a magnetic hysteresis loop (Figure 17), is crucial for the evaluation of the possibility of material for external magnetic field separation.

For unmodified spinel ferrites NPs, the saturation magnetization value fluctuates around 70-90 Am^2/kg, depending on M cation type [165–167]. The Ms values decrease after increasing the percentage of non-magnetic compound in the nanocomposite.

In the recent literature reports, even up to 9–10 reuse cycles with almost no loss in photocatalytic activity have been observed for G-based magnetic nanocomposites [146,168,169]. Recycled photocatalysts, before reusing in the next photodegradation process, are often recovered by simple washing with demineralized water and drying [170] up to alkaline solution treatment [171].

Table 4. Summary of selected graphene-magnetic NPs photocatalysts.

Photocatalyst	Pollutants	Experimental Conditions	Findings	Ref.
$Co_{0.7}Zn_{0.3}Er_xFe_{2-x}O_4$-rGO (x = 0.01–0.05)	MB	1-h vis (Xe lamp)	100% dec.; 55% deg.	[173]
AFG@MIL-101(Fe) (amine-func. Fe_3O_4 wrapped with rGO)	DIZ, ATZ pesticides	HPHg (400 W, λ = 546.8); 30 ppm; 105 min	100% rem. (DIZ, alk. pH), 81% rem. (ATZ, aci. pH); TOC rem.; 4 cycles—almost same act.	[174]
$ZnO/ZnFe_2O_4$/N-doped G $ZnO/CoFe_2O_4$/N-doped G	MO MG	10-W LED (400–700 nm); 10 ppm; 70 min (MG), 140 min (MO)	99% rem. $ZnO/CoFe_2O_4$/N-doped G (pH 4–6). 10 cycles—almost same act.	[175]
$BiFeO_3$-G (G: 1–9 wt%)	MO	SSol (200-W Xe lamp); 10 ppm; 6 h	50% MO deg. on $BiFeO_3$-5%G; e^- captured by G, h^+ oxidative species	[149]
Fe_2O_3-Fe_3O_4-M-G (M—montmorillonite)	MO	vis (300-W Xe lamp); 20 ppm	100% MO deg. (175 min) on Fe_2O_3-Fe_3O_4-M-G; 98.8% recycling with magnetic field	[176]
$BiFeO_3$-g-GNS	MOMB	vis (λ ≥ 420 nm, 300-W halogen lamps); 20 ppm; 60 min	87% deg. MB, 35.9% deg. MO; activity increase with increase of $BiFeO_3$ content on GNS	[177]
$CoFe_2O_4$-G (G = 15–50%)	MB, RhB, MO, BL-G, RGB	vis (500-W Xe lamp, JB450 cut-off filter; 20 ppm; 240 min	95% deg. MB on $CoFe_2O_4$-G(40%)	[178]
$MgFe_2O_4$-G	MB	UV/vis; 40 min	~100% deg. MB	[179]
GO/magnetite/Ce-doped TiO_2	TC	vis (300-W Xe lamp, 400-nm cut-off filter); 25 ppm; 60 min.	89.92% deg. on MGO-Ce-TiO_2; 4 cycles-decrease activity to 60%	[180]
Fe_2TiO_5/rGO_x (x = 0–15%)	MB	vis (50-W LED); 10 ppm; 150 min	40% deg. on Fe_2TiO_5/rGO_x (x = 10%)	[181]

aci.—acidic; act.—activity; alk.—alkaline; ATZ—atrazine; BL-G—active black; dec.—decoloration; deg.—degradation; DIZ—diazinon; funct.—functionalized; GNS—graphene nanosheets; MB—Methylene Blue, MG—Malachite Green; MO—Methyl Orange; RGB—active red; RhB—Rhodamine B; SSol—simulated solar light; TC—tetracycline.

In summary, it is clear that coupling of graphene and its composite with magnetic particles might results in efficient, stable and easily separable photocatalyst for various environmental application.
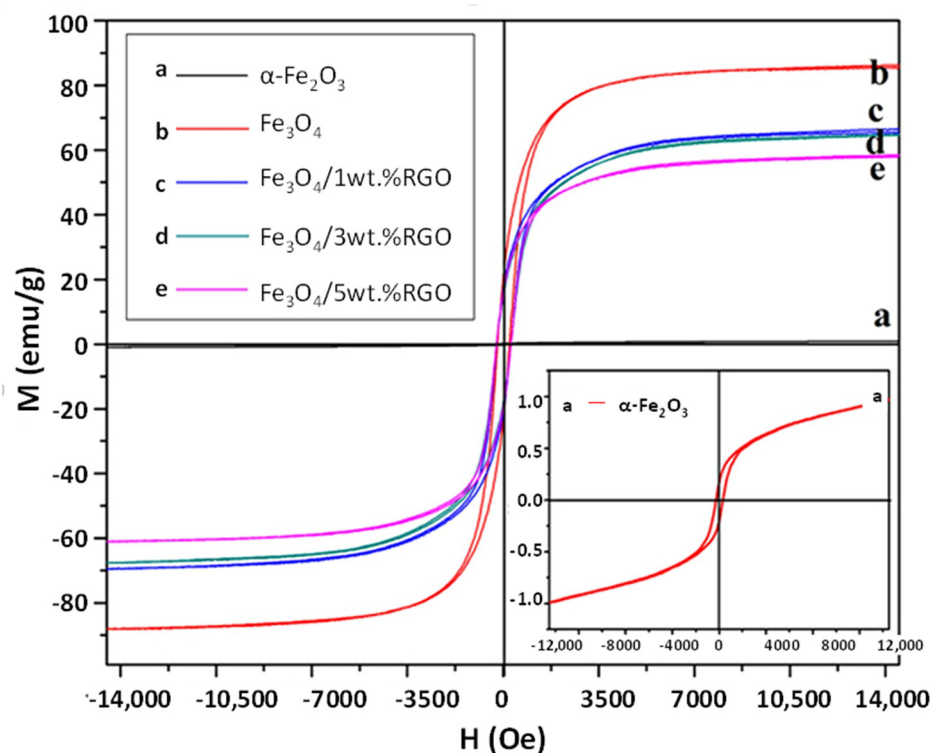
Figure 17. Fe_3O_4/G nanocomposites saturation magnetization values presented as hysteresis loops. Reprinted with permission from [172]. Copyright (2016) Creative Commons Attribution.

4. Summary and Conclusions

This review summarizes the present state of knowledge about the structural and application issues of the presence of graphene as an important part of composites with the semiconducting metal oxides in their promising forms, such as faceted particles, various morphological particulate systems and photonic crystals. The incorporation of graphene into mentioned composites is responsible for the introduction of unique properties such as improvement of charge carriers transfer, including exceptional enhancement of electron-hole separation, and also the extension of light absorption properties towards visible region of solar spectrum. Furthermore, the improvement of adsorption capacity for reagents participating in the photocatalytic reactions, resulting from the presence of graphene structures, is also important for an increase in the overall photocatalytic performance. The enhancement of photocatalytic properties originates also from the synergistic effects between the presence of specified morphological form of novel photocatalysts, such as faceted particles, nanotubes/nanowires, opal/inverse opal (slow photon effect) and graphene, or the simultaneous presence of semiconductor modifier or semiconductors' heterojunction system combined with graphene. Moreover, the coupling of G/GO/rGO with ferromagnet particles, such as Fe, Co, Zn, Bi etc. ferrites oxides, does not only increase the photocatalytic activity due to charge carriers separation and more efficient light harvesting, but also allows the recycling and reusing of the photocatalysts. Undemanding separation in external magnetic field fits perfectly into the green chemistry trend due to limitation of post-process photocatalysts' waste and energy costs. Despite the fact that the number of studies on graphene-based photocatalysts is constantly growing, some details describing the mechanism of their exceptional photocatalytic activities are not still entirely clear. Therefore, more research on this topic is needed to clarify this issue, and to enable the design of more efficient, stable and reusable photocatalytic graphene-based materials with a wide application potential, especially in the field of environmental aspects.

For application purposes, the antimicrobial activity of graphene and its derivatives are very attractive as they might be used in fight against viruses, bacteria (including antibiotic

resistant strains), yeast or filamentous fungi. However, the mechanism has not been clearly understood yet, and there are some concerns about the cytotoxicity against higher animals and human cells. For that reason, the primary objective of follow-up study should be the research conducted in parallel on advance scientific understanding on the mechanisms of action at the biochemical or molecular level. A complete understanding of that issue might create great opportunities to develop the smart bandages or wound dressing against particular pathogens. Moreover, graphene-based materials provide a potentially promising tool for real-time diagnostics of the pathogen population or cancer cells in each patient that enables the development of new target therapies. Other possible applications are engineered biomaterials with high biocompatibility and long-life medical devices, such as body implants (teeth and bones).

Author Contributions: Writing—original draft preparation, M.J., M.E.-K., Z.W., Z.B., T.R.M., T.M.K., K.W., A.M.-S. and E.K.; Writing—review and editing, M.J., M.E.-K., Z.W., Z.B., T.R.M., T.M.K., K.W., A.M.-S. and E.K. All authors have read and agreed to the published version of the manuscript.

Institutional Review Board Statement: Not applicable.

Informed Consent Statement: Not applicable.

Data Availability Statement: Data available in a publicly accessible repository.

Conflicts of Interest: The authors declare no conflict of interest.

References

1. Hoffmann, M.R.; Martin, S.T.; Choi, W.Y.; Bahnemann, D.W. Environmental applications of semiconductor photocatalysis. *Chem. Rev.* **1995**, *95*, 69–96. [CrossRef]
2. Wang, K.L.; Janczarek, M.; Wei, Z.S.; Raja-Mogan, T.; Endo-Kimura, M.; Khedr, T.M.; Ohtani, B.; Kowalska, E. Morphology- and crystalline composition-governed activity of titania-based photocatalysts: Overview and perspective. *Catalysts* **2019**, *9*, 1054. [CrossRef]
3. Zaleska, A. Doped-TiO_2: A review. *Rec. Pat. Eng.* **2008**, *2*, 157–164. [CrossRef]
4. Lambert, T.N.; Chavez, C.A.; Hernandez-Sachez, B.; Lu, P.; Bell, N.S.; Ambrosini, A.; Friedman, T.; Boyle, T.J.; Wheeler, D.R.; Hubert, D.L. Synthesis and Characterization of Titania-Graphene Nanocomposites. *J. Phys. Chem. C* **2009**, *113*, 19812–19823. [CrossRef]
5. Kim, S.R.; Parvez, M.K.; Chhowalla, M. UV-reduced of graphene oxide and its application as an interfacial layer to reduce the back-transport reactions in dye-sensitized solar cells. *Chem. Phys. Lett.* **2009**, *483*, 124–127. [CrossRef]
6. Williams, G.; Seger, B.; Kamat, P.V. TiO_2-Graphene Nanocomposites. UV-Assisted Photocatalytic Reduction of Graphene Oxide. *ACS Nano* **2008**, *2*, 1487–1491. [CrossRef]
7. Bai, X.; Zhang, X.Y.; Hua, Z.L.; Ma, W.Q.; Dai, Z.Y.; Huang, X.; Gu, H.X. Uniformly distributed anatase TiO_2 nanoparticles on graphene: Synthesis, characterization, and photocatalytic application. *J. Alloys Compd.* **2014**, *599*, 10–18. [CrossRef]
8. Li, F.; Du, P.H.; Liu, W.; Li, X.S.; Ji, H.D.; Duan, J.; Zhao, D.Y. Hydrothermal synthesis of graphene grafted titania/titanate nanosheets for photocatalytic degradation of 4-chlorophenol: Solar-light-driven photocatalytic activity and computational chemistry analysis. *Chem. Eng. J.* **2018**, *331*, 685–694. [CrossRef]
9. Stengl, V.; Bakardjieva, S.; Grygar, T.M.; Bludska, J.; Kormunda, M. TiO_2-graphene oxide nanocomposite as advanced photocatalytic materials. *Chem. Cent. J.* **2013**, *7*, 41. [CrossRef]
10. Nagaraju, G.; Ebeling, G.; Goncalves, R.V.; Teixeira, S.R.; Weibel, D.E.; Dupont, J. Controlled growth of TiO_2 and TiO_2-RGO composite nanoparticles in ionic liquids for enhanced photocatalytic H_2 generation. *J. Mol. Catal. A Chem.* **2013**, *378*, 213–220. [CrossRef]
11. Wang, K.L.; Endo-Kimura, M.; Belchi, R.; Zhang, D.; Habert, A.; Boucle, J.; Ohtani, B.; Kowalska, E.; Herlin-Boime, N. Carbon/graphene-modified titania with enhanced photocatalytic activity under UV and vis irradiation. *Materials* **2019**, *12*, 4158. [CrossRef]
12. Neelgund, G.M.; Oki, A. Graphene-Coupled ZnO: A Robust NIR-Induced Catalyst for Rapid Photo-Oxidation of Cyanide. *ACS Omega* **2017**, *2*, 9095–9102. [CrossRef]
13. Wang, X.W.; Li, Q.C.; Zhou, C.X.; Cao, Z.Q.; Zhang, R.B. ZnO rod/reduced graphene oxide sensitized by alpha-Fe_2O_3 nanoparticles for effective visible-light photoreduction of CO_2. *J. Colloid Interface Sci.* **2019**, *554*, 335–343. [CrossRef]

14. Giovannetti, R.; Rommozzi, E.; Zannotti, M.; D'Amato, C.A. Recent Advances in Graphene Based TiO$_2$ Nanocomposites (GTiO$_2$Ns) for Photocatalytic Degradation of Synthetic Dyes. *Catalysts* **2017**, *7*, 305. [CrossRef]

15. Wei, Z.; Janczarek, M.; Wang, K.; Zheng, S.; Kowalska, E. Morphology-governed performance of plasmonic photocatalysts. *Catalysts* **2020**, *10*, 1070. [CrossRef]

16. Selloni, A. Crystal growth—Anatase shows its reactive side. *Nat. Mater.* **2008**, *7*, 613–615. [CrossRef] [PubMed]

17. Yang, H.G.; Sun, C.H.; Qiao, S.Z.; Zou, J.; Liu, G.; Smith, S.C.; Cheng, H.M.; Lu, G.Q. Anatase TiO$_2$ single crystals with a large percentage of reactive facets. *Nature* **2008**, *453*, 638–641. [CrossRef]

18. Janczarek, M.; Kowalska, E.; Ohtani, B. Decahedral-shaped anatase titania photocatalyst particles: Synthesis in a newly developed coaxial-flow gas-phase reactor. *Chem. Eng. J.* **2016**, *289*, 502–512. [CrossRef]

19. Wei, Z.; Janczarek, M.; Endo, M.; Wang, K.L.; Balcytis, A.; Nitta, A.; Mendez-Medrano, M.G.; Colbeau-Justin, C.; Juodkazis, S.; Ohtani, B.; et al. Noble metal-modified faceted anatase titania photocatalysts: Octahedron versus decahedron. *Appl. Catal. B Environ.* **2018**, *237*, 574–587. [CrossRef]

20. Wei, Z.; Kowalska, E.; Verrett, J.; Colbeau-Justin, C.; Remita, H.; Ohtani, B. Morphology-dependent photocatalytic activity of octahedral anatase particles prepared by ultrasonication-hydrothermal reaction of titanates. *Nanoscale* **2015**, *7*, 12392–12404. [CrossRef]

21. Amano, F.; Prieto-Mahaney, O.O.; Terada, Y.; Yasumoto, T.; Shibayama, T.; Ohtani, B. Decahedral single-crystalline particles of anatase titanium(IV) oxide with high photocatalytic activity. *Chem. Mater.* **2009**, *21*, 2601–2603. [CrossRef]

22. Amano, F.; Yasumoto, T.; Prieto-Mahaney, O.O.; Uchida, S.; Shibayama, T.; Ohtani, B. Photocatalytic activity of octahedral single-crystalline mesoparticles of anatase titanium(IV) oxide. *Chem. Commun.* **2009**, *17*, 2311–2313. [CrossRef]

23. Amano, F.; Yasumoto, T.; Mahaney, O.O.P.; Uchida, S.; Shibayama, T.; Terada, Y.; Ohtani, B. Highly Active Titania Photocatalyst Particles of Controlled Crystal Phase, Size, and Polyhedral Shapes. *Top. Catal.* **2010**, *53*, 455–461. [CrossRef]

24. Sofianou, M.V.; Psycharis, V.; Boukos, N.; Vaimakis, T.; Yu, J.G.; Dillert, R.; Bahnemann, D.; Trapalis, C. Tuning the photocatalytic selectivity of TiO2 anatase nanoplates by altering the exposed crystal facets content. *Appl. Catal. B Environ.* **2013**, *142*, 761–768. [CrossRef]

25. Dozzi, M.V.; Selli, E. Specific Facets-Dominated Anatase TiO$_2$: Fluorine-Mediated Synthesis and Photoactivity. *Catalysts* **2013**, *3*, 455–485. [CrossRef]

26. Murakami, N.; Kurihara, Y.; Tsubota, T.; Ohno, T. Shape-Controlled Anatase Titanium(IV) Oxide Particles Prepared by Hydrothermal Treatment of Peroxo Titanic Acid in the Presence of Polyvinyl Alcohol. *J. Phys. Chem. C* **2009**, *113*, 3062–3069. [CrossRef]

27. Su, Y.; Li, H.F.; Ma, H.B.; Robertson, J.; Nathan, A. Controlling surface termination and facet orientation in Cu$_2$O nanoparticles for high photocatalytic activity: A combined experimental and density functional theory study. *ACS Appl. Mater. Interfaces* **2017**, *9*, 8100–8106. [CrossRef] [PubMed]

28. Chen, T.N.; Kao, J.C.; Zhong, X.Y.; Chan, S.J.; Patra, A.S.; Lo, Y.C.; Huang, M.H. Facet-specific photocatalytic activity enhancement of Cu$_2$O polyhedra functionalized with 4-ethynylanaline resulting from band structure tuning. *ACS Cent. Sci.* **2020**, *6*, 984–994. [CrossRef] [PubMed]

29. Liu, T.F.; Zhao, Q.Y.; Li, C.; Lyu, Y.; Dupuis, M. Photocatalytic facet selectivity in BiVO$_4$ nanoparticles: Polaron electronic structure and thermodynamic stability considerations for photocatalysis. *J. Phys. Chem. C* **2019**, *123*, 20142–20151. [CrossRef]

30. Lardhi, S.; Cavallo, L.; Harb, M. Significant impact of exposed facets on the BiVO$_4$ material performance for photocatalytic water splitting reactions. *J. Phys. Chem. Lett.* **2020**, *11*, 5497–5503. [CrossRef]

31. Wang, X.W.; Wang, W.Y.; Miao, Y.Q.; Feng, G.; Zhang, R.B. Facet-selective photodeposition of gold nanoparticles on faceted ZnO crystals for visible light photocatalysis. *J. Colloid Interface Sci.* **2016**, *475*, 112–118. [CrossRef]

32. Yu, Z.Z.; Zhan, B.W.; Ge, B.H.; Zhu, Y.T.; Dai, Y.; Zhou, G.J.; Yu, F.P.; Wang, P.; Huang, B.B.; Zhan, J. Synthesis of high efficient and stable plasmonic photocatalyst Ag/AgNbO$_3$ with specific exposed crystal-facets and intimate heterogeneous interface via combustion route. *Appl. Surf. Sci.* **2019**, *488*, 485–493. [CrossRef]

33. Warmuth, L.; Ritschel, C.; Feldmann, C. Facet-, composition- and wavelength-dependent photocatalysis of Ag$_2$MoO$_4$. *RSC Adv.* **2020**, *10*, 18377–18383. [CrossRef]

34. Dong, F.; Xiong, T.; Yan, S.; Wang, H.Q.; Sun, Y.J.; Zhang, Y.X.; Huang, H.W.; Wu, Z.B. Facets and defects cooperatively promote visible light plasmonic photocatalysis with Bi nanowires@BiOCl nanosheets. *J. Catal.* **2016**, *344*, 401–410. [CrossRef]

35. Zhang, L.; Wang, W.Z.; Sun, S.M.; Jiang, D.; Gao, E.P. Selective transport of electron and hole among {001} and {110} facets of BiOCl for pure water splitting. *Appl. Catal. B Environ.* **2015**, *162*, 470–474. [CrossRef]

36. Liu, G.; Yu, J.C.; Lu, G.Q.; Cheng, H.M. Crystal facet engineering of semiconductor photocatalysts: Motivations, advances and unique properties. *Chem. Commun.* **2011**, *47*, 6763–6783. [CrossRef] [PubMed]

37. Jiang, B.J.; Tian, C.G.; Pan, Q.J.; Jiang, Z.; Wang, J.Q.; Yan, W.S.; Fu, H.G. Enhanced photocatalytic activity and electron transfer mechanisms of graphene/TiO$_2$ with exposed {001} facets. *J. Phys. Chem. C* **2011**, *115*, 23718–23725. [CrossRef]

38. Zhao, Y.L.; Wei, Y.C.; Wu, X.X.; Zheng, H.L.; Zhao, Z.; Liu, J.; Li, J.M. Graphene-wrapped Pt/TiO$_2$ photocatalysts with enhanced photogenerated charges separation and reactant adsorption for high selective photoreduction of CO$_2$ to CH$_4$. *Appl. Catal. B Environ.* **2018**, *226*, 360–372. [CrossRef]

39. Wang, C.; Meng, D.L.; Sun, J.H.; Memon, J.; Huang, Y.; Geng, J.X. Graphene wrapped TiO$_2$ based catalysts with enhanced photocatalytic activity. *Adv. Mater. Interfaces* **2014**, *1*, 1. [CrossRef]

40. Liu, H.; Liu, S.; Zhang, Z.L.; Dong, X.N.; Liu, T.T. Hydrothermal etching fabrication of TiO$_2$@graphene hollow structures: Mutually independent exposed {001} and {101} facets nanocrystals and its synergistic photocaltalytic effects. *Sci. Rep.* **2016**, *6*, 33839. [CrossRef]

41. Wei, Q.; Wang, Y.; Qin, H.Y.; Wu, J.M.; Lu, Y.F.; Chi, H.Z.; Yang, F.; Zhou, B.; Yu, H.L.; Liu, J.B. Construction of rGO wrapping octahedral Ag-Cu$_2$O heterostructure for enhanced visible light photocatalytic activity. *Appl. Catal. B Environ.* **2018**, *227*, 132–144. [CrossRef]

42. Wang, T.; Li, C.J.; Ji, J.Y.; Wei, Y.J.; Zhang, P.; Wang, S.P.; Fan, X.B.; Gong, J.L. Reduced graphene oxide (rGO)/BiVO$_4$ composites with maximized interfacial coupling for visible lght photocatalysis. *ACS Sustain. Chem. Eng.* **2014**, *2*, 2253–2258. [CrossRef]

43. Wang, H.; Lu, J.R.; Liu, L.; Cui, W.Q.; Liang, Y.H. Ultra-thin rGO nanosheet modified TiO$_2$ nanotube arrays for boosted photoelectrochemical performance. *Appl. Surf. Sci.* **2020**, *506*, 144966. [CrossRef]

44. Pan, X.; Zhao, Y.; Liu, S.; Korzeniewski, C.L.; Wang, S.; Fan, Z.Y. Comparing graphene-TiO$_2$ nanowire and graphene-TiO$_2$ nanoparticle composite photocatalysts. *ACS Appl. Mater. Interfaces* **2012**, *4*, 3944–3950. [CrossRef] [PubMed]

45. Wang, M.G.; Han, J.; Xiong, H.X.; Guo, R.; Yin, Y.D. Nanostructured hybrid shells of r-GO/AuNP/m-TiO$_2$ as highly active photocatalysts. *ACS Appl. Mater. Interfaces* **2015**, *7*, 6909–6918. [CrossRef]

46. Yablonovitch, E. Photonic Band-Gap Structures. *J. Opt. Soc. Am. B* **1993**, *10*, 283–295. [CrossRef]

47. Lima, A.W.; Sombra, A.S.B. Graphene-photonic crystal switch. *Opt. Commun.* **2014**, *321*, 150–156. [CrossRef]

48. Raja-Mogan, T.; Ohtani, B.; Kowalska, E. Photonic crystals for plasmonic photocatalysis. *Catalysts* **2020**, *10*, 827. [CrossRef]

49. Khaleque, A.; Hattori, H.T. Absorption enhancement in graphene photonic crystal structures. *Appl. Opt.* **2016**, *55*, 2936–2942. [CrossRef]

50. Chen, K.; Zhou, X.; Cheng, X.; Qiao, R.X.; Cheng, Y.; Liu, C.; Xie, Y.D.; Yu, W.T.; Yao, F.R.; Sun, Z.P.; et al. Graphene photonic crystal fibre with strong and tunable light-matter interaction. *Nat. Photonics* **2019**, *13*, 754–759. [CrossRef]

51. Pourmahmoud, V.; Rezaei, B. Manipulation of Bragg and graphene photonic band gaps in one-dimensional photonic crystal containing graphene. *Optik* **2019**, *185*, 875–880. [CrossRef]

52. Dash, J.N.; Jha, R. Graphene-based birefringent photonic crystal fiber sensor using surface plasmon resonance. *IEEE Photonic Technol. Lett.* **2014**, *26*, 1092–1095. [CrossRef]

53. Sreekanth, K.V.; Zeng, S.W.; Yong, K.T.; Yu, T. Sensitivity enhanced biosensor using graphene-based one-dimensional photonic crystal. *Sens. Actuators B Chem.* **2013**, *182*, 424–428. [CrossRef]

54. Papadakis, D.; Diamantopoulou, A.; Pantazopoulos, P.A.; Palles, D.; Sakellis, E.; Boukos, N.; Stefanou, N.; Likodimos, V. Nanographene oxide-TiO$_2$ photonic films as plasmon-free substrates for surface-enhanced Raman scattering. *Nanoscale* **2019**, *11*, 21542–21553. [CrossRef]

55. Apostolaki, M.A.; Toumazatou, A.; Antoniadou, M.; Sakellis, E.; Xenogiannopoulou, E.; Gardelis, S.; Boukos, N.; Falaras, P.; Dimoulas, A.; Likodimos, V. Graphene quantum dot-TiO$_2$ photonic crystal films for photocatalytic applications. *Nanomaterials* **2020**, *10*, 2566. [CrossRef]

56. Diamantopoulou, A.; Sakellis, E.; Gardelis, S.; Tsoutsou, D.; Glenis, S.; Boukos, N.; Dimoulas, A.; Likodimos, V. Advanced photocatalysts based on reduced nanographene oxide-TiO$_2$ photonic crystal films. *Materials* **2019**, *12*, 2518. [CrossRef]

57. Baghbadorani, H.K.; Barvestani, J.; Entezar, S.R. Biosensors based on Bloch surface waves in one-dimensional photonic crystal with graphene nanolayers. *Appl. Opt.* **2017**, *56*, 462–469. [CrossRef]

58. Gan, X.T.; Mak, K.F.; Gao, Y.D.; You, Y.M.; Hatami, F.; Hone, J.; Heinz, T.F.; Englund, D. Strong enhancement of light-matter interaction in graphene coupled to a photonic crystal nanocavity. *Nano Lett.* **2012**, *12*, 5626–5631. [CrossRef]

59. Ghasemi, F.; Entezar, S.R.; Razi, S. Graphene based photonic crystal optical filter: Design and exploration of the tunability. *Phys. Lett. A* **2019**, *383*, 2551–2560. [CrossRef]

60. Zeng, S.W.; Yong, K.T.; Roy, I.; Dinh, X.Q.; Yu, X.; Luan, F. A Review on functionalized gold nanoparticles for biosensing applications. *Plasmonics* **2011**, *6*, 491–506. [CrossRef]

61. Homola, J. Present and future of surface plasmon resonance biosensors. *Anal. Bioanal. Chem.* **2003**, *377*, 528–539. [CrossRef] [PubMed]

62. Khurgin, J.B.; Boltasseva, A. Reflecting upon the losses in plasmonics and metamaterials. *MRS Bull.* **2012**, *37*, 768–779. [CrossRef]

63. Jovic, V.; Idriss, H.; Waterhouse, G.I.N. Slow photon amplification of gas-phase ethanol photo-oxidation in titania inverse opal photonic crystals. *Chem. Phys.* **2016**, *479*, 109–121. [CrossRef]

64. Curti, M.; Mendive, C.B.; Grela, M.A.; Bahnemann, D.W. Stopband tuning of TiO$_2$ inverse opals for slow photon absorption. *Mater. Res. Bull.* **2017**, *91*, 155–165. [CrossRef]

65. Liu, J.T.; Liu, N.H.; Li, J.; Li, X.J.; Huang, J.H. Enhanced absorption of graphene with one-dimensional photonic crystal. *Appl. Phys. Lett.* **2012**, *101*, 052104. [CrossRef]

66. Zhang, K.; Shi, X.; Kim, J.K.; Lee, J.S.; Park, J.H. Inverse opal structured alpha-Fe$_2$O$_3$ on graphene thin films: Enhanced photo-assisted water splitting. *Nanoscale* **2013**, *5*, 1939–1944. [CrossRef] [PubMed]

67. Yoon, K.Y.; Lee, J.S.; Kim, K.; Bak, C.H.; Kim, S.I.; Kim, J.B.; Jang, J.H. Hematite-based photoelectrochemical water splitting supported by inverse opal structures of graphene. *ACS Appl. Mater. Interfaces* **2014**, *6*, 22634–22639. [CrossRef] [PubMed]

68. Huo, J.W.; Yuan, C.; Wang, Y. Nanocomposites of three-dimensionally ordered porous TiO$_2$ decorated with Pt and reduced graphene oxide for the visible-light photocatalytic degradation of waterborne pollutants. *ACS Appl. Nano Mater.* **2019**, *2*, 2713–2724. [CrossRef]

69. Boppella, R.; Kochuveedu, S.T.; Kim, H.; Jeong, M.J.; Mota, F.M.; Park, J.H.; Kim, D.H. Plasmon-sensitized graphene/TiO$_2$ inverse opal nanostructures with enhanced charge collection efficiency for water splitting. *ACS Appl. Mater. Interfaces* **2017**, *9*, 7075–7083. [CrossRef] [PubMed]

70. Chen, L.C.; Xie, L.Z.; Wang, M.Z.; Ge, X.W. Preparation of three-dimensional inverse opal SnO$_2$/graphene composite microspheres and their enhanced photocatalytic activities. *J. Mater. Chem. A* **2015**, *3*, 2991–2998. [CrossRef]

71. Diamantopoulou, A.; Sakellis, E.; Romanos, G.E.; Gardelis, S.; Ioannidis, N.; Boukos, N.; Falaras, P.; Likodimos, V. Titania photonic crystal photocatalysts functionalized by graphene oxide nanocolloids. *Appl. Catal. B Environ.* **2019**, *240*, 277–290. [CrossRef]

72. Wang, W.X.; Wang, X.X.; Xing, J.L.; Gong, Q.B.; Wang, H.H.; Wang, J.J.; Chen, Z.; Ai, Y.J.; Wang, X.K. Multi-heteroatom doped graphene-like carbon nanospheres with 3D inverse opal structure: A promising bisphenol-A remediation material. *Environ. Sci. Nano* **2019**, *6*, 809–819. [CrossRef]

73. Raja-Mogan, T.; Lehoux, A.; Takashima, M.; Kowalska, E.; Ohtani, B. Slow photon-induced enhancement of photocatalytic activity of gold nanoparticle-incorporated titania in-verse opal. *Chem. Lett.* **2021**, in press. [CrossRef]

74. Yao, Y.; Chen, Z.; Zhang, A.J.; Zhu, J.H.; Wei, X.R.; Guo, J.; Wu, W.D.; Chen, D.; Wu, Z.X. Surface-coating synthesis of nitrogen-doped inverse opal carbon materials with ultrathin micro/mesoporous graphene-like walls for oxygen reduction and supercapacitors. *J. Mater. Chem. A* **2017**, *5*, 25237–25248. [CrossRef]

75. Chen, J.I.L.; Loso, E.; Ebrahim, N.; Ozin, G.A. Synergy of slow photon and chemically amplified photochemistry in platinum nanocluster-loaded inverse titania opals. *J. Am. Chem. Soc.* **2008**, *130*, 5420–5421. [CrossRef] [PubMed]

76. Zhao, Y.X.; Yang, B.F.; Xu, J.; Fu, Z.P.; Wu, M.; Li, F. Facile synthesis of Ag nanoparticles supported on TiO$_2$ inverse opal with enhanced visible-light photocatalytic activity. *Thin Solid Films* **2012**, *520*, 3515–3522. [CrossRef]

77. Chwalibog, A.; Sawosz, E.; Hotowy, A.; Szeliga, J.; Mitura, S.; Mitura, K.; Grodzik, M.; Orlowski, P.; Sokolowska, A. Visualization of interaction between inorganic nanoparticles and bacteria or fungi. *Int. J. Nanomed.* **2010**, *5*, 1085–1094. [CrossRef]

78. Sambhy, V.; MacBride, M.M.; Peterson, B.R.; Sen, A. Silver bromide nanoparticle/polymer composites: Dual action tunable antimicrobial materials. *J. Am. Chem. Soc.* **2006**, *128*, 9798–9808. [CrossRef] [PubMed]

79. Sunada, K.; Minoshima, M.; Hashimoto, K. Highly efficient antiviral and antibacterial activities of solid-state cuprous compounds. *J. Hazard. Mater.* **2012**, *235*, 265–270. [CrossRef]

80. Matsunaga, T.; Tomoda, R.; Nakajima, T.; Wake, H. Photoelectrochemical sterilization of microbial-cells by semiconductor powders. *FEMS Microbiol. Lett.* **1985**, *29*, 211–214. [CrossRef]

81. McEvoy, J.G.; Zhang, Z.S. Antimicrobial and photocatalytic disinfection mechanisms in silver-modified photocatalysts under dark and light conditions. *J. Photochem. Photobiol. C* **2014**, *19*, 62–75. [CrossRef]

82. Markowska-Szczupak, A.; Ulfig, K.; Morawski, W.A. The application of titanium dioxide for deactivation of bioparticulates: An overview. *Catal. Today* **2011**, *161*, 249–257. [CrossRef]

83. Mitoraj, D.; Janczyk, A.; Strus, M.; Kisch, H.; Stochel, G.; Heczko, P.B.; Macyk, W. Visible light inactivation of bacteria and fungi by modified titanium dioxide. *Photochem. Photobiol. Sci.* **2007**, *6*, 642–648. [CrossRef] [PubMed]

84. Markowska-Szczupak, A.; Wang, K.L.; Rokicka, P.; Endo, M.; Wei, Z.S.; Ohtani, B.; Morawski, A.W.; Kowalska, E. The effect of anatase and rutile crystallites isolated from titania P25 photocatalyst on growth of selected mould fungi. *J. Photochem. Photobiol. B* **2015**, *151*, 54–62. [CrossRef]

85. Markowska-Szczupak, A.; Endo-Kimura, M.; Paszkiewicz, O.; Kowalska, E. Are titania photocatalysts and titanium implants safe? Review on the toxicity of titanium compounds. *Nanomaterials* **2020**, *10*, 2065. [CrossRef]

86. Akhavan, O.; Ghaderi, E. Photocatalytic reduction of graphene oxide nanosheets on TiO$_2$ thin film for photoinactivation of bacteria in solar light irradiation. *J. Phys. Chem. C* **2009**, *113*, 20214–20220. [CrossRef]

87. Akhavan, O.; Ghaderi, E. Toxicity of graphene and graphene oxide nanowalls against bacteria. *ACS Nano* **2010**, *4*, 5731–5736. [CrossRef]

88. Khanam, P.N.; Hasan, A. Biosynthesis and characterization of graphene by using non-toxic reducing agent from *Allium Cepa* extract: Anti-bacterial properties. *Int. J. Biol. Macromol.* **2019**, *126*, 151–158. [CrossRef]

89. Palmieri, V.; Bugli, F.; Lauriola, M.C.; Cacaci, M.; Torelli, R.; Ciasca, G.; Conti, C.; Sanguinetti, M.; Papi, M.; De Spirito, M. Bacteria meet graphene: Modulation of graphene oxide nanosheet interaction with human pathogens for effective antimicrobial therapy. *ACS Biomater. Sci. Eng.* **2017**, *3*, 619–627. [CrossRef]

90. Jira, J.; Rezek, B.; Kriha, V.; Artemenko, A.; Matolinova, I.; Skakalova, V.; Stenclova, P.; Kromka, A. Inhibition of *E. coli* growth by nanodiamond and graphene oxide enhanced by Luria-Bertani medium. *Nanomaterials* **2018**, *8*, 140. [CrossRef]

91. Gusev, A.; Zakharova, O.; Muratov, D.S.; Vorobeva, N.S.; Sarker, M.; Rybkin, I.; Bratashov, D.; Kolesnikov, E.; Lapanje, A.; Kuznetsov, D.V.; et al. Medium-dependent antibacterial properties and bacterial filtration ability of reduced graphene oxide. *Nanomaterials* **2019**, *9*, 1454. [CrossRef]

92. Li, X.F.; Sun, J.Z.; Che, Y.L.; Lv, Y.; Liu, F. Antibacterial properties of chitosan chloride-graphene oxide composites modified quartz sand filter media in water treatment. *Int. J. Biol. Macromol.* **2019**, *121*, 760–773. [CrossRef] [PubMed]

93. Alayande, A.B.; Chae, S.; Kim, I.S. Surface morphology-dependent spontaneous bacterial behaviors on graphene oxide membranes. *Sep. Purif. Technol.* **2019**, *226*, 68–74. [CrossRef]

94. Biswas, K.; De, D.; Bandyopadhyay, J.; Sen, P. Differential antibacterial response exhibited by graphene nanosheets toward gram-positive bacterium *Staphylococcus aureus*. *IET Nanobiotechnol.* **2018**, *12*, 733–740. [CrossRef] [PubMed]

95. Liu, S.B.; Zeng, T.H.; Hofmann, M.; Burcombe, E.; Wei, J.; Jiang, R.R.; Kong, J.; Chen, Y. Antibacterial activity of graphite, graphite oxide, graphene oxide, and reduced graphene oxide: Membrane and oxidative stress. *ACS Nano* **2011**, *5*, 6971–6980. [CrossRef]

96. Krishnamoorthy, K.; Veerapandian, M.; Zhang, L.H.; Yun, K.; Kim, S.J. Antibacterial efficiency of graphene nanosheets against pathogenic bacteria via lipid peroxidation. *J. Phys. Chem. C* **2012**, *116*, 17280–17287. [CrossRef]

97. Li, J.H.; Wang, G.; Zhu, H.Q.; Zhang, M.; Zheng, X.H.; Di, Z.F.; Liu, X.Y.; Wang, X. Antibacterial activity of large-area monolayer graphene film manipulated by charge transfer. *Sci. Rep.* **2014**, *4*, 4359. [CrossRef]

98. Nguyen, H.N.; Chaves-Lopez, C.; Oliveira, R.C.; Paparella, A.; Rodrigues, D.E. Cellular and metabolic approaches to investigate the effects of graphene and graphene oxide in the fungi *Aspergillus flavus* and *Aspergillus niger*. *Carbon* **2019**, *143*, 419–429. [CrossRef]

99. Di Giulio, M.; Zappacosta, R.; Di Lodovico, S.; Di Campli, E.; Siani, G.; Fontana, A.; Cellini, L. Antimicrobial and antibiofilm efficacy of graphene oxide against chronic wound microorganisms. *Antimicrob. Agents Chemother.* **2018**, *62*, e00547-18. [CrossRef] [PubMed]

100. Diez-Orejas, R.; Feito, M.J.; Cicuendez, M.; Casarrubios, L.; Rojo, J.M.; Portoles, M.T. Graphene oxide nanosheets increase *Candida albicans* killing by pro-inflammatory and reparative peritoneal macrophages. *Colloid Surfaces B* **2018**, *171*, 250–259. [CrossRef]

101. Gandhi, P.R.; Chandramohan, G. Preparation of novel chitosan-graphene oxide/tin oxide nanocomposites for anti-bacterial activities. *Dig. J. Nanomater. Biostruct.* **2020**, *15*, 561–568.

102. Yang, M.C.; Tseng, Y.Q.; Liu, K.H.; Cheng, Y.W.; Chen, W.T.; Chen, W.T.; Hsiao, C.W.; Yung, M.C.; Hsu, C.C.; Liu, T.Y. Preparation of amphiphilic chitosan-graphene oxide-cellulose nanocrystalline composite hydrogels and their biocompatibility and antibacterial properties. *Appl. Sci.* **2019**, *9*, 3051. [CrossRef]

103. Bandara, P.C.; Nadres, E.T.; Pena-Bahamonde, J.; Rodrigues, D.F. Impact of water chemistry, shelf-life, and regeneration in the removal of different chemical and biological contaminants in water by a model polymeric graphene oxide nanocomposite membrane coating. *J. Water Process. Eng.* **2019**, *32*, 100967. [CrossRef]

104. Bugli, F.; Cacaci, M.; Palmieri, V.; Di Santo, R.; Torelli, R.; Ciasca, G.; Di Vito, M.; Vitali, A.; Conti, C.; Sanguinetti, M.; et al. Curcumin-loaded graphene oxide flakes as an effective antibacterial system against methicillin-resistant *Staphylococcus aureus*. *Interface Focus* **2018**, *8*, 20170059. [CrossRef]

105. Ghorbanzadeh, R.; Assadian, H.; Chiniforush, N.; Parker, S.; Pourakbari, B.; Ehsani, B.; Alikhani, M.Y.; Bahador, A. Modulation of virulence in *Enterococcus faecalis* cells surviving antimicrobial photodynamic inactivation with reduced graphene oxide-curcumin: An ex vivo biofilm model. *Photodiagnosis Photodyn. Ther.* **2020**, *29*, 101643. [CrossRef] [PubMed]

106. De Maio, F.; Palmieri, V.; Santarelli, G.; Perini, G.; Salustri, A.; Palucci, I.; Sali, M.; Gervasoni, J.; Primiano, A.; Ciasca, G.; et al. Graphene oxide-linezolid combination as potential new anti-tuberculosis treatment. *Nanomaterials* **2020**, *10*, 1431. [CrossRef]

107. Gao, Y.; Wu, J.C.; Ren, X.M.; Tan, X.L.; Hayat, T.; Alsaedi, A.; Cheng, C.; Chen, C.L. Impact of graphene oxide on the antibacterial activity of antibiotics against bacteria. *Environ. Sci. Nano* **2017**, *4*, 1016–1024. [CrossRef]

108. Ramasamy, M.; Nanda, S.S.; Lee, J.H.; Lee, J. Construction of alizarin conjugated graphene oxide composites for inhibition of *Candida albicans* biofilms. *Biomolecules* **2020**, *10*, 565. [CrossRef] [PubMed]

109. Goy, R.C.; de Britto, D.; Assis, O.B.G. A review of the antimicrobial activity of chitosan. *Polimeros* **2009**, *19*, 241–247. [CrossRef]

110. Helander, I.M.; Nurmiaho-Lassila, E.L.; Ahvenainen, R.; Rhoades, J.; Roller, S. Chitosan disrupts the barrier properties of the outer membrane of Gram-negative bacteria. *Int. J. Food Microbiol.* **2001**, *71*, 235–244. [CrossRef]

111. Lee, J.H.; Kim, Y.G.; Ryu, S.Y.; Lee, J. Calcium-chelating alizarin and other anthraquinones inhibit biofilm formation and the hemolytic activity of *Staphylococcus aureus*. *Sci. Rep.* **2016**, *6*, 19267. [CrossRef] [PubMed]

112. Manoharan, R.K.; Lee, J.H.; Kim, Y.G.; Lee, J. Alizarin and Chrysazin inhibit biofilm and hyphal formation by *Candida albicans*. *Front. Cell. Infect. Microbiol.* **2017**, *7*, 447. [CrossRef] [PubMed]

113. Naeem, H.; Ajmal, M.; Qureshi, R.B.; Muntha, S.T.; Farooq, M.; Siddiq, M. Facile synthesis of graphene oxide-silver nanocomposite for decontamination of water from multiple pollutants by adsorption, catalysis and antibacterial activity. *J. Environ. Manag.* **2019**, *230*, 199–211. [CrossRef] [PubMed]

114. Peng, J.M.; Lin, J.C.; Chen, Z.Y.; Wei, M.C.; Fu, Y.X.; Lu, S.S.; Yu, D.S.; Zhao, W. Enhanced antimicrobial activities of silver-nanoparticle-decorated reduced graphene nanocomposites against oral pathogens. *Mater. Sci. Eng. C* **2017**, *71*, 10–16. [CrossRef]

115. Ko, K.; Kim, M.J.; Lee, J.Y.; Kim, W.; Chung, H. Effects of graphene oxides and silver-graphene oxides on aquatic microbial activity. *Sci. Total Environ.* **2019**, *651*, 1087–1095. [CrossRef]

116. Cobos, M.; De-La-Pinta, I.; Quindos, G.; Fernandez, M.J.; Fernandez, M.D. Graphene oxide-silver nanoparticle nanohybrids: Synthesis, characterization, and antimicrobial properties. *Nanomaterials* **2020**, *10*, 376. [CrossRef] [PubMed]

117. Cobos, M.; De-La-Pinta, I.; Quindos, G.; Fernandez, M.J.; Fernandez, M.D. Synthesis, physical, mechanical and antibacterial properties of nanocomposites based on poly(vinyl alcohol)/graphene oxide-silver nanoparticles. *Polymers* **2020**, *12*, 723. [CrossRef]

118. Agarwalla, S.V.; Ellepola, K.; da Costa, M.C.F.; Fechine, G.J.M.; Morin, J.L.P.; Neto, A.H.C.; Seneviratne, C.J.; Rosa, V. Hydrophobicity of graphene as a driving force for inhibiting biofilm formation of pathogenic bacteria and fungi. *Dent. Mater.* **2019**, *35*, 403–413. [CrossRef] [PubMed]

119. Arshad, A.; Iqbal, J.; Mansoor, Q. NiO-nanoflakes grafted graphene: An excellent photocatalyst and a novel nanomaterial for achieving complete pathogen control. *Nanoscale* **2017**, *9*, 16321–16328. [CrossRef]

120. Kozuszko, S.N.; Sanchez, M.A.; de Ferro, M.I.G.; Sfer, A.M.; Madrid, A.P.M.; Takabatake, K.; Nakano, K.; Nagatsuka, H.; Rodriguez, A.P. Antibacterial activity and biocompability of zinc oxide and graphite particles as endodontic materials. *J. Hard Tissue Biol.* **2017**, *26*, 311–318. [CrossRef]

121. Ghanem, A.F.; Badawy, A.A.; Mohram, M.E.; Rehim, M.H.A. Synergistic effect of zinc oxide nanorods on the photocatalytic performance and the biological activity of graphene nano sheets. *Heliyon* **2020**, *6*, e03283. [CrossRef] [PubMed]

122. Ficociello, G.; De Canis, M.G.; Trillo, G.; Cavallini, D.; Santo, M.S.; Uccelletti, D.; Mancini, P. Anti-candidal activity and in vitro cytotoxicity assessment of graphene nanoplatelets decorated with zinc oxide nanorods. *Nanomaterials* **2018**, *8*, 752. [CrossRef]

123. Jiang, G.F.; Li, X.F.; Che, Y.L.; Lv, Y.; Liu, F.; Wang, Y.Q.; Zhao, C.C.; Wang, X.J. Antibacterial and anticorrosive properties of CuZnO@RGO waterborne polyurethane coating in circulating cooling water. *Environ. Sci. Pollut. Res.* **2019**, *26*, 9027–9040. [CrossRef] [PubMed]

124. Dhanasekar, M.; Jenefer, V.; Nambiar, R.B.; Babu, S.G.; Selvam, S.P.; Neppolian, B.; Bhat, S.V. Ambient light antimicrobial activity of reduced graphene oxide supported metal doped TiO$_2$ nanoparticles and their PVA based polymer nanocomposite films. *Mater. Res. Bull.* **2018**, *97*, 238–243. [CrossRef]

125. Liu, Y.; Zeng, X.K.; Hu, X.Y.; Hu, J.; Wang, Z.Y.; Yin, Y.C.; Sun, C.H.; Zhang, X.W. Two-dimensional g-C$_3$N$_4$/TiO$_2$ nanocomposites as vertical Z-scheme heterojunction for improved photocatalytic water disinfection. *Catal. Today* **2019**, *335*, 243–251. [CrossRef]

126. Cruz-Ortiz, B.R.; Hamilton, J.W.J.; Pablos, C.; Diaz-Jimenez, L.; Cortes-Hernandez, D.A.; Sharma, P.K.; Castro-Alferez, M.; Fernandez-Ibanez, P.; Dunlop, P.S.M.; Byrne, J.A. Mechanism of photocatalytic disinfection using titania-graphene composites under UV and visible irradiation. *Chem. Eng. J.* **2017**, *316*, 179–186. [CrossRef]

127. Luo, R.; Xu, Z.Y.; Lin, X.M. Preparation and characterisation of silver nanoparticles in an aqueous suspension of TETA modified graphene oxide and their antibacterial activity. *Micro Nano Lett.* **2018**, *13*, 369–373. [CrossRef]

128. Cobos, M.; De-La-Pinta, I.; Quindos, G.; Fernandez, M.J.; Fernandez, M.D. One-step eco-friendly synthesized silver-graphene oxide/poly(vinyl alcohol) antibacterial nanocomposites. *Carbon* **2019**, *150*, 101–116. [CrossRef]

129. Xu, W.R.; Xie, W.J.; Huang, X.Q.; Chen, X.; Huang, N.; Wang, X.; Liu, J. The graphene oxide and chitosan biopolymer loads TiO$_2$ for antibacterial and preservative research. *Food Chem.* **2017**, *221*, 267–277. [CrossRef]

130. Zhang, H.; Lv, X.J.; Li, Y.M.; Wang, Y.; Li, J.H. P25-graphene composite as a high performance photocatalyst. *ACS Nano* **2010**, *4*, 380–386. [CrossRef] [PubMed]

131. Paszkiwicz-Gawron, M.; Kowalska, E.; Endo-Kimura, M.; Zwara, J.; Pancielejko, A.; Wang, K.; Lisowski, W.; Luczak, J.; Zaleska-Medynska, A.; Gerabowska-Musial, E. Stannates, titanates and tantalates modified with carbon and graphene quantum dots for enhancement of visible-light photocatalytic activity. *Appl. Surf. Sci.* **2021**, *541*, 148425. [CrossRef]

132. Whitehead, K.A.; Vaidya, M.; Liauw, C.M.; Brownson, D.A.C.; Ramalingam, P.; Kamieniak, J.; Rowley-Neale, S.J.; Tetlow, L.A.; Wilson-Nieuwenhuis, J.S.T.; Brown, D.; et al. Antimicrobial activity of graphene oxide-metal hybrids. *Int. Biodeterior. Biodegrad.* **2017**, *123*, 182–190. [CrossRef]

133. Pulingam, T.; Thong, K.L.; Ali, M.E.; Appaturi, J.N.; Dinshaw, I.J.; Ong, Z.Y.; Leo, B.F. Graphene oxide exhibits differential mechanistic action towards Gram-positive and Gram-negative bacteria. *Colloids Surf. B* **2019**, *181*, 6–15. [CrossRef] [PubMed]

134. Stanford, M.G.; Li, J.T.; Chen, Y.D.; McHugh, E.A.; Liopo, A.; Xiao, H.; Tour, J.M. Self-sterilizing laser-induced graphene bacterial air filter. *ACS Nano* **2019**, *13*, 11912–11920. [CrossRef] [PubMed]

135. Srivastava, A.K.; Dwivedi, N.; Dhand, C.; Khan, R.; Sathish, N.; Gupta, M.K.; Kumar, R.; Kumar, S. Potential of graphene-based materials to combat COVID-19: Properties, perspectives, and prospects. *Mater. Today Chem.* **2020**, *18*, 100385. [CrossRef]

136. Alegret, N.; Criado, A.; Prato, M. Recent advances of graphene-based hybrids with magnetic nanoparticles for biomedical applications. *Curr. Med. Chem.* **2017**, *24*, 529–536. [CrossRef]

137. Orfanakis, G.; Patila, M.; Catzikonstantinou, A.V.; Lyra, K.M.; Kouloumpis, A.; Spyrou, K.; Katapodis, P.; Paipetis, A.; Rudolf, P.; Gournis, D.; et al. Hybrid nanomaterials of magnetic iron nanoparticles and graphene oxide as matrices for the immobilization of beta-glucosidase: Synthesis, characterization, and biocatalytic properties. *Front. Mater.* **2018**, *5*, 25. [CrossRef]

138. Xu, K.J.; Wang, Y.Z.; Ding, X.Q.; Huang, Y.H.; Li, N.; Wen, Q. Magnetic solid-phase extraction of protein with deep eutectic solvent immobilized magnetic graphene oxide nanoparticles. *Talanta* **2016**, *148*, 153–162. [CrossRef]

139. Kim, S.E.; Tieu, M.V.; Hwang, S.Y.; Lee, M.H. Magnetic particles: Their applications from sample preparations to biosensing platforms. *Micromachines* **2020**, *11*, 302. [CrossRef]

140. Mishra, A.K.; Ramaprabhu, S. Ultrahigh arsenic sorption using iron oxide-graphene nanocomposite supercapacitor assembly. *J. Appl. Phys.* **2012**, *112*, 104315. [CrossRef]

141. Kim, S.; Park, C.M.; Jang, M.; Son, A.; Her, N.; Yu, M.; Snyder, S.; Kim, D.H.; Yoon, Y. Aqueous removal of inorganic and organic contaminants by graphene-based nanoadsorbents: A review. *Chemosphere* **2018**, *212*, 1104–1124. [CrossRef]

142. Zhang, Y.; Chen, B.A.; Zhang, L.M.; Huang, J.; Chen, F.H.; Yang, Z.P.; Yao, J.L.; Zhang, Z.J. Controlled assembly of Fe$_3$O$_4$ magnetic nanoparticles on graphene oxide. *Nanoscale* **2011**, *3*, 1446–1450. [CrossRef]

143. Xiang, Q.J.; Yu, J.G.; Jaroniec, M. Graphene-based semiconductor photocatalysts. *Chem. Soc. Rev.* **2012**, *41*, 782–796. [CrossRef]

144. Fu, Y.S.; Chen, Q.; He, M.Y.; Wan, Y.H.; Sun, X.Q.; Xia, H.; Wang, X. Copper ferrite-graphene hybrid: A multifunctional heteroarchitecture for photocatalysis and energy storage. *Ind. Eng. Chem. Res.* **2012**, *51*, 11700–11709. [CrossRef]

145. Cheng, R.L.; Fan, X.Q.; Wang, M.; Li, M.L.; Tian, J.J.; Zhang, L.X. Facile construction of CuFe$_2$O$_4$/g-C$_3$N$_4$ photocatalyst for enhanced visible-light hydrogen evolution. *RSC Adv.* **2016**, *6*, 18990–18995. [CrossRef]

146. Hosseini, S.M.; Hosseini-Monfared, H.; Abbasi, V. Silver ferrite-graphene nanocomposite and its good photocatalytic performance in air and visible light for organic dye removal. *Appl. Organomet. Chem.* **2017**, *31*, e3589. [CrossRef]

147. Mrotek, E.; Dudziak, S.; Malinowska, I.; Pelczarski, S.; Ryzynska, Z.; Zielinska-Jurek, A. Improved degradation of etodolac in the presence of core-shell $ZnFe_2O_4/SiO_2/TiO_2$ magnetic photocatalyst. *Sci. Total. Environ.* **2020**, *724*, 138167. [CrossRef]

148. Zielinska-Jurek, A.; Bielan, Z.; Wysocka, I.; Strychalska, J.; Janczarek, M.; Klimczuk, T. Magnetic semiconductor photocatalysts for the degradation of recalcitrant chemicals from flow back water. *J. Environ. Manag.* **2017**, *195*, 157–165. [CrossRef]

149. Dai, J.F.; Xian, T.; Di, L.J.; Yang, H. Preparation of $BiFeO_3$-graphene nanocomposites and their enhanced photocatalytic activities. *J. Nanomater.* **2013**, *2013*, 642897. [CrossRef]

150. Beydoun, D.; Amal, R.; Low, G.K.C.; McEvoy, S. Novel photocatalyst: Titania-coated magnetite. Activity and photodissolution. *J. Phys. Chem. B* **2000**, *104*, 4387–4396. [CrossRef]

151. Bavarsiha, F.; Rajabi, M.; Montazeri-Pour, M. Synthesis of $SrFe_{12}O_{19}/SiO_2/TiO_2$ composites with core/shell/shell nano-structure and evaluation of their photo-catalytic efficiency for degradation of methylene blue. *J. Mater. Sci. Mater. Electron.* **2018**, *29*, 1877–1887. [CrossRef]

152. Park, C.M.; Kim, Y.M.; Kim, K.H.; Wang, D.J.; Su, C.M.; Yoon, Y. Potential utility of graphene-based nano spinel ferrites as adsorbent and photocatalyst for removing organic/inorganic contaminants from aqueous solutions: A mini review. *Chemosphere* **2019**, *221*, 392–402. [CrossRef] [PubMed]

153. Bao, N.Z.; Shen, L.M.; Wang, Y.H.; Padhan, P.; Gupta, A. A facile thermolysis route to monodisperse ferrite nanocrystals. *J. Am. Chem. Soc.* **2007**, *129*, 12374–12375. [CrossRef] [PubMed]

154. Naskar, A.; Khan, H.; Jana, S. One pot low temperature synthesis of graphene coupled Gd-doped $ZnFe_2O_4$ nanocomposite for effective removal of antibiotic levofloxacin drug. *J. Sol-Gel Sci. Technol.* **2018**, *86*, 599–609. [CrossRef]

155. Yamaguchi, N.U.; Bergamasco, R.; Hamoudi, S. Magnetic $MnFe_2O_4$-graphene hybrid composite for efficient removal of glyphosate from water. *Chem. Eng. J.* **2016**, *295*, 391–402. [CrossRef]

156. Luciano, A.J.R.; Soletti, L.D.; Ferreira, M.E.C.; Cusioli, L.F.; de Andrade, M.B.; Bergamasco, R.; Yamaguchi, N.U. Manganese ferrite dispersed over graphene sand composite for methylene blue photocatalytic degradation. *J. Environ. Chem. Eng.* **2020**, *8*, 104191. [CrossRef]

157. Jelokhani, F.; Sheibani, S.; Ataie, A. Adsorption and photocatalytic characteristics of cobalt ferrite-reduced graphene oxide and cobalt ferrite-carbon nanotube nanocomposites. *J. Photochem. Photobiol. A* **2020**, *403*, 112867. [CrossRef]

158. Sharma, R.; Bansal, S.; Singhal, S. Tailoring the photo-Fenton activity of spinel ferrites (MFe_2O_4) by incorporating different cations (M = Cu, Zn, Ni and Co) in the structure. *RSC Adv.* **2015**, *5*, 6006–6018. [CrossRef]

159. Gan, L.; Shang, S.M.; Yuen, C.W.M.; Jiang, S.X.; Hu, E.L. Hydrothermal synthesis of magnetic $CoFe_2O_4$/graphene nanocomposites with improved photocatalytic activity. *Appl. Surf. Sci.* **2015**, *351*, 140–147. [CrossRef]

160. Chen, P. Synthesis and photocatalysis of novel magnetic reduced graphene oxide-$ZnFe_2O_4$ nanocomposites with highly efficient interface-induced effect. *J. Sol-Gel Sci. Technol.* **2017**, *82*, 397–406. [CrossRef]

161. Zhang, Q.; Zhang, Y.H.; Meng, Z.L.; Tong, W.S.; Yu, X.L.; An, Q. Constructing the magnetic bifunctional graphene/titania nanosheet-based composite photocatalysts for enhanced visible-light photodegradation of MB and electrochemical ORR from polluted water. *Sci. Rep.* **2017**, *7*, 12296. [CrossRef]

162. Houshiar, M.; Zebhi, F.; Razi, Z.J.; Alidoust, A.; Askari, Z. Synthesis of cobalt ferrite ($CoFe_2O_4$) nanoparticles using combustion, coprecipitation, and precipitation methods: A comparison study of size, structural, and magnetic properties. *J. Magn. Magn. Mater.* **2014**, *371*, 43–48. [CrossRef]

163. Lee, J.S.; Cha, J.M.; Yoon, H.Y.; Lee, J.K.; Kim, Y.K. Magnetic multi-granule nanoclusters: A model system that exhibits universal size effect of magnetic coercivity. *Sci. Rep.* **2015**, *5*, 12135. [CrossRef]

164. Wu, W.; Jiang, C.Z.; Roy, V.A.L. Recent progress in magnetic iron oxide-semiconductor composite nanomaterials as promising photocatalysts. *Nanoscale* **2015**, *7*, 38–58. [CrossRef]

165. Andersen, H.L.; Saura-Muzquiz, M.; Granados-Miralles, C.; Canevet, E.; Lock, N.; Christensen, M. Crystalline and magnetic structure-property relationship in spinel ferrite nanoparticles. *Nanoscale* **2018**, *10*, 14902–14914. [CrossRef]

166. Aslibeiki, B.; Kameli, P.; Ehsani, M.H.; Salamati, H.; Muscas, G.; Agostinelli, E.; Foglietti, V.; Casciardi, S.; Peddis, D. Solvothermal synthesis of $MnFe_2O_4$ nanoparticles: The role of polymer coating on morphology and magnetic properties. *J. Magn. Magn. Mater.* **2016**, *399*, 236–244. [CrossRef]

167. Dey, S.; Dey, S.K.; Majumder, S.; Poddar, A.; Dasgupta, P.; Banerjee, S.; Kumar, S. Superparamagnetic behavior of nanosized Co0.2Zn0.8Fe2O4 synthesized by a flow rate controlled chemical coprecipitation method. *Physica B* **2014**, *448*, 247–252. [CrossRef]

168. Rani, G.J.; Rajan, M.A.J.; Kumar, G.G. Reduced graphene oxide/$ZnFe_2O_4$ nanocomposite as an efficient catalyst for the photocatalytic degradation of methylene blue dye. *Res. Chem. Intermed.* **2017**, *43*, 2669–2690. [CrossRef]

169. Wu, L.K.; Wu, H.; Zhang, H.B.; Cao, H.Z.; Hou, G.Y.; Tang, Y.P.; Zheng, G.Q. Graphene oxide/$CuFe_2O_4$ foam as an efficient absorbent for arsenic removal from water. *Chem. Eng. J.* **2018**, *334*, 1808–1819. [CrossRef]

170. Wang, X.Y.; Wang, A.Q.; Ma, J. Visible-light-driven photocatalytic removal of antibiotics by newly designed C_3N_4@$MnFe_2O_4$-graphene nanocomposites. *J. Hazard. Mater.* **2017**, *336*, 81–92. [CrossRef] [PubMed]

171. Santhosh, C.; Kollu, P.; Felix, S.; Velmurugan, V.; Jeong, S.K.; Grace, A.N. $CoFe_2O_4$ and $NiFe_2O_4$@graphene adsorbents for heavy metal ions—Kinetic and thermodynamic analysis. *RSC Adv.* **2015**, *5*, 28965–28972. [CrossRef]

172. Yin, Y.C.; Zeng, M.; Liu, J.; Tang, W.K.; Dong, H.R.; Xia, R.Z.; Yu, R.H. Enhanced high-frequency absorption of anisotropic Fe_3O_4/graphene nanocomposites. *Sci. Rep.* **2016**, *6*, 25075. [CrossRef]

173. Mahmood, M.; Yousuf, M.A.; Baig, M.M.; Imran, M.; Suleman, M.; Shahid, M.; Khan, M.A.; Warsi, M.F. Spinel ferrite magnetic nanostructures at the surface of graphene sheets for visible light photocatalysis applications. *Physica B* **2018**, *550*, 317–323. [CrossRef]

174. Fakhri, H.; Farzadkia, M.; Boukherroub, R.; Srivastava, V.; Sillanpaa, M. Design and preparation of core-shell structured magnetic graphene oxide@MIL-101(Fe): Photocatalysis under shell to remove diazinon and atrazine pesticides. *Sol. Energy* **2020**, *208*, 990–1000. [CrossRef]

175. Chandel, N.; Sharma, K.; Sudhaik, A.; Raizada, P.; Hosseini-Bandegharaei, A.; Thakur, V.K.; Singh, P. Magnetically separable $ZnO/ZnFe_2O_4$ and $ZnO/CoFe_2O_4$ photocatalysts supported onto nitrogen doped graphene for photocatalytic degradation of toxic dyes. *Arab. J. Chem.* **2020**, *13*, 4324–4340. [CrossRef]

176. Wang, J.; Chen, Y.; Liu, G.J.; Cao, Y. Synthesis, characterization and photocatalytic activity of inexpensive and non-toxic Fe_2O_3-Fe_3O_4 nano-composites supported by montmorillonite and modified by graphene. *Compos. Part B Eng.* **2017**, *114*, 211–222. [CrossRef]

177. Bajpai, O.P.; Mandal, S.; Ananthakrishnan, R.; Mandal, P.; Khastgir, D.; Chattopadhyay, S. Structural features, magnetic properties and photocatalytic activity of bismuth ferrite nanoparticles grafted on graphene nanosheets. *New J. Chem.* **2018**, *42*, 10712–10723. [CrossRef]

178. Fu, Y.S.; Chen, H.Q.; Sun, X.Q.; Wang, X. Combination of cobalt ferrite and graphene: High-performance and recyclable visible-light photocatalysis. *Appl. Catal. B Environ.* **2012**, *111*, 280–287. [CrossRef]

179. Shakir, I.; Sarfraz, M.; Ali, Z.; Aboud, M.F.A.; Agboola, P.O. Magnetically separable and recyclable graphene-$MgFe_2O_4$ nanocomposites for enhanced photocatalytic applications. *J. Alloys Compd.* **2016**, *660*, 450–455. [CrossRef]

180. Cao, M.H.; Wang, P.F.; Ao, Y.H.; Wang, C.; Hou, J.; Qian, J. Visible light activated photocatalytic degradation of tetracycline by a magnetically separable composite photocatalyst: Graphene oxide/magnetite/cerium-doped titania. *J. Colloid Interface Sci.* **2016**, *467*, 129–139. [CrossRef] [PubMed]

181. Guediri, M.K.; Chebli, D.; Bouguettoucha, A.; Bourzami, R.; Amrane, A. Novel Fe_2TiO_5/reduced graphene oxide heterojunction photocatalyst with improved adsorption capacity and visible light photoactivity: Experimental and DFT approach. *Environ. Sci. Pollut. Res.* **2021**, *28*, 8507–8519. [CrossRef] [PubMed]